Advances in Colloid and Interface Science 246 (2017) 133–152

Contents lists available at ScienceDirect

Advances in Colloid and Interface Science

journal homepage: www.elsevier.com/locate/cis

Historical perspective

A review on the mechanical and thermodynamic robustness of superhydrophobic surfaces

Liam R.J. Scarratt[a], Ullrich Steiner[b], Chiara Neto[a,*]

[a] School of Chemistry, Australian Institute for Nanoscale Science and Technology, The University of Sydney, NSW 2006, Australia
[b] Adolphe Merkle Institute, University of Fribourg, Chemin des Verdiers 4, CH-1700 Fribourg, Switzerland

ARTICLE INFO

Keywords:
Superhydrophobic surfaces
Mechanical robustness
Plastron stability
Roughness
Mechanical testing
Cassie state

ABSTRACT

Advancements in the fabrication and study of superhydrophobic surfaces have been significant over the past 10 years, and some 20 years after the discovery of the lotus effect, the study of special wettability surfaces can be considered mainstream. While the fabrication of superhydrophobic surfaces is well advanced and the physical properties of superhydrophobic surfaces well-understood, the robustness of these surfaces, both in terms of mechanical and thermodynamic properties, are only recently getting attention in the literature. In this review we cover publications that appeared over the past ten years on the thermodynamic and mechanical robustness of superhydrophobic surfaces, by which we mean the long term stability under conditions of wear, shear and pressure. The review is divided into two parts, the first dedicated to thermodynamic robustness and the second dedicated to mechanical robustness of these complex surfaces. Our work is intended as an introductory review for researchers interested in addressing longevity and stability of superhydrophobic surfaces, and provides an outlook on outstanding aspects of investigation.

1. Introduction

The fabrication of robust superhydrophobic coatings that are extremely water repellent and resist stains would have far reaching practical applications, however their manufacture is yet to be fully accomplished [1]. Since the characterization of the Lotus leaf [2], there have been thousands of publications presenting methods for the fabrication of artificial superhydrophobic surfaces on which water droplets cannot spread, forming a contact angle larger than 150°. The hallmark of superhydrophobicity is the motion of drops on the surface: they roll across the surface [3–5], rather than spreading or sliding as with liquids that have lower contact angles with the surface [6]. The rolling of drops relies on the combination of micro-scale and nano-scale surface roughness [7], which traps pockets of air [1]. The facile motion of the drops on the surface, combined with the low adhesion of particulate dirt on the rough apolar surfaces, provides a very efficient cleaning mechanism, hence the “self-cleaning” moniker. This wetting scenario is known as the Cassie-Baxter state (CB) or Cassie state [8], characterized by low adhesion of water droplets on the surface, and is of technological interest due to its potential to benefit drag-reducing, anti-fouling and self-cleaning surface coatings [9].

The work by Lafuma and Quéré illustrated that the lifetime of the trapped air (plastron) varies with the structural details and surface energy of the superhydrophobic surface [10]. For a superhydrophobic surface to be more stable in a Cassie state, the critical angle θ_c at which air remains trapped below the drop on a composite surface must be small, where $\cos\theta_c = (\varphi_s - 1) / (r - \varphi_s)$, with r the ratio of the actual over the apparent surface area of the substrate and φ_s the fraction of solid in contact with the liquid. A very rough surface may exist or transition into a Wenzel wetting state when the air escapes out of the roughness, and the liquid comes in contact directly with the roughness. Air pockets are stable in the Cassie state only if the contact angle is larger than θ_c. Therefore θ_c must be as small as possible for the Cassie state surface to be thermodynamically stable. Indeed the superhydrophobic lotus leaf has a large value of roughness r, due to having both micro and nano-scale roughness.

Thermodynamic and kinetic robustness refers to the stability of the air trapped on the surface (so-called plastron) in the Cassie state, and its ability to resist transitioning to a Wenzel wetting state (where the air escapes out of the roughness) [1]. The thermodynamic stability of the plastron is of critical importance to applications of superhydrophobic surfaces, because when the surface features are filled with water, the surface loses its water repellent properties, and may become stickier than smooth surfaces. Water can penetrate into the roughness through the vapor phase by local condensation, or by application of high pressure, through droplet impact, droplet evaporation, high Laplace

* Corresponding author.
E-mail address: chiara.neto@sydney.edu.au (C. Neto).

http://dx.doi.org/10.1016/j.cis.2017.05.018

Available online 30 May 2017

pressure or hydrostatic pressure [11].

The potential of superhydrophobic surfaces to reduce ice accumulation have been proposed as useful in airplane wings and other applications [12]. Their drag-reducing properties have been proposed for use in a number of other energy-related applications. However, the implementation of superhydrophobic surfaces is limited by the thermodynamic and mechanical fragility of their hierarchical surface roughness [10,11,13–20], and the high production costs involved [21].

In the following Sections we first review studies investigating the thermodynamic robustness of the Cassie superhydrophobic state, then the most established methods to fabricate superhydrophobic surfaces, focusing on a critical comparison of the anticipated mechanical robustness produced by the different methods. The reviewed methods include: lithography and templating, plasma and chemical etching, chemical deposition, colloidal assembly and layer by layer deposition, electrospinning and electrospraying. We then cover other emerging fabrication methods, such as surface wrinkling, and self-healing surfaces. In the latter category, we touch briefly on liquid-infused surfaces, which are already positioned to replace superhydrophobic coatings because of their ability to self-repair and their customizability. Finally, we review methods to test chemical and mechanical robustness, focusing on the techniques that are suitable to study highly structured and rough surfaces.

2. Thermodynamic and kinetic robustness

In the following Section, we refer to the thermodynamic and kinetic robustness as the stability of the Cassie wetting state under equilibrium wetting conditions in air or underwater, and when exposed to external forces including mechanical energy and droplet impact, respectively.

While the wettability of surfaces is often classified into either Wenzel or Cassie wetting, it is important to emphasize that both wetting states constitute minima in the overall free energy of the drop, which is (in the absence of gravity) determined by the surface fractions of the liquid drop in contact with the solid and air, and the integral surface curvature. Apart from the question of which of these two free energy minima is lower, the thermodynamic transition between the two is of considerable practical interest. For example, a system for which Wenzel wetting is thermodynamically favored can be practically useful if the energetic barrier between the Cassie state and the Wenzel state is high. Conversely, superhydrophobic surfaces with energetically favored Cassie wetting are problematic, if the transition to the Wenzel local minimum in the free energy is facile, since the recovery from the Wenzel state is kinetically problematic (see below) and local Wenzel wetting can lead to the frequent pinning of the drop.

The transition between the two wetting states requires (*i*) the local motion of the contact line, locally spreading the liquid front from one state to the other, and (*ii*) the escape or ingress of air, destroying or re-establishing the plastron, respectively. The role of the local contact angle in the wetting equilibrium was first recognized by Johnson and Dettre [22], who for a sinusoidal surface roughness analyzed the transition from Wenzel to Cassie (CB) wetting in terms of the local slope of the surface (Fig. 1). Cassie -wetting is obtained when spreading of the microscopic contact line of a suspended drop would require to exceed Young's contact angle (i.e. the equilibrium contact angle of the liquid on a perfectly planar surface) [23], making this process thermodynamically unfavorable. Note that this geometrical argument is not based on the overall free energy of the drop, and does therefore not allow determining the free energy of the Wenzel and Cassie wetted states, but it illustrates the existence of a free energy barrier between the two. The local pinning of the contact line allows the creation of surfaces which are superhydrophobic and superoleophobic at the same time, as beautifully demonstrated by Tutejaa et al. [5]. For model surfaces, such as sinusoidal roughness [24] or pillar arrays [1], the energy barrier between Cassie and Wenzel wetting can be analytically determined. For more complex surface morphologies, numerical approaches are required.

Instead of classifying liquids on surfaces in terms of the two wetting regimes, it is therefore more useful to consider them as energetic states. The coexistence of Wenzel and Cassie wetting has been demonstrated numerous times [1] (Fig. 2a). Extending a model by Marmur [25], the free energy landscape of drops on surfaces can be calculated, as shown in Fig. 2b [5], quantifying the free energies of Wenzel and Cassie wetting and the energetic barrier between them. Drops are typically trapped in either of these two states, and the exact state may depend on the details of how the system is prepared as shown in Fig. 2a.

The energetic barrier can be overcome by the application of an additional force, the simplest of which is droplet impact [1,26,27]. Mechanically vibrating the surface can also induce a Cassie to Wenzel transition [28], so can the evaporation of the drops [29,30], as illustrated in Fig. 3.

Note that even for high energy barriers, metastable wetting states are robust only on structurally homogeneous surfaces, since local defects in the surface structure may initiate the transition of the entire drop from a metastable Cassie into a thermodynamically preferred Wenzel state. This adds to the general problem of defect sensitivity of Cassie-surfaces (the most prevalent being the pinning of Cassie-drops on surface defects), making their practical implementation difficult.

The requirement of air removal for the transition from Cassie to Wenzel wetting, or reestablishment of the plastron for the reverse process, can be subdivided into two aspects, related to the morphology of the surface and the thermodynamic stability of the plastron. Regarding the substrate morphology, most implementations of superhydrophobic surfaces exhibit a sufficient lateral porosity for the air to escape during the Cassie to Wenzel transition. In fact, laterally enclosed plastrons would violate the main requirement of the Cassie state by the formation of a microscopically continuous liquid-solid contact line, which pins the drop [31]. However, the reverse process, the formation of a plastron by air ingress under the drop is much more difficult. It is hindered by the fact that the microscopic water contact line has to move (spread) under the drop, which is a process that is easily arrested by pinning. This can be overcome by the application of an additional force helping contact line retraction, either through the in-coupling of mechanical energy, e.g. by vibrating the surface [32,33].

In 2000, Herminghaus described that the plastron disappears from Lotus leaves when submerged at a depth of 20 cm for a few seconds [34]. When removed, the surface was clearly in the Wenzel state. This effect was later more systematically studied for natural and manufactured superhydrophobic surfaces [31,35], as shown in Fig. 4. This indicates that while the plastron can be quite stable when the surface is exposed to small amounts of liquids, it is unstable under water. While standard wetting theories assume the thermodynamic coexistence of three inert, immiscible phases (gas, liquid, solid), air is however partially miscible in water. When submerged, the plastron is hydrostatically pressurized and the air is dissolved in the water. This has been quantitatively studied for Teflon surfaces with a hierarchical roughness [13], describing a two-stage plastron decay consisting of the thinning of the extended plastron followed by the break-up and decay of the plastron into pinned surface bubbles (Fig. 5). This late stage can be described by adapting the Epstein-Plesset formalism [36] for the stability of gas bubbles to the plastron. However, a quantitative prediction of plastron stability is complicated by the fact that water and air are rarely in thermodynamic equilibrium under ambient conditions. This has triggered a range of studies on the underwater stability of plastrons [37,38].

Switching from Wenzel to Cassie wetting is significantly more difficult, as this would require the water to be removed from the holes or grooves in the surface and a gas evolution mechanism which replenishes the plastron, such as by gas or vapor generation [39–41], local pressure regulation [42–44], vibrations [33]. Gas evolution has for example been achieved by water electrolysis, which requires the incorporation of an electrode into the superhydrophobic surface and

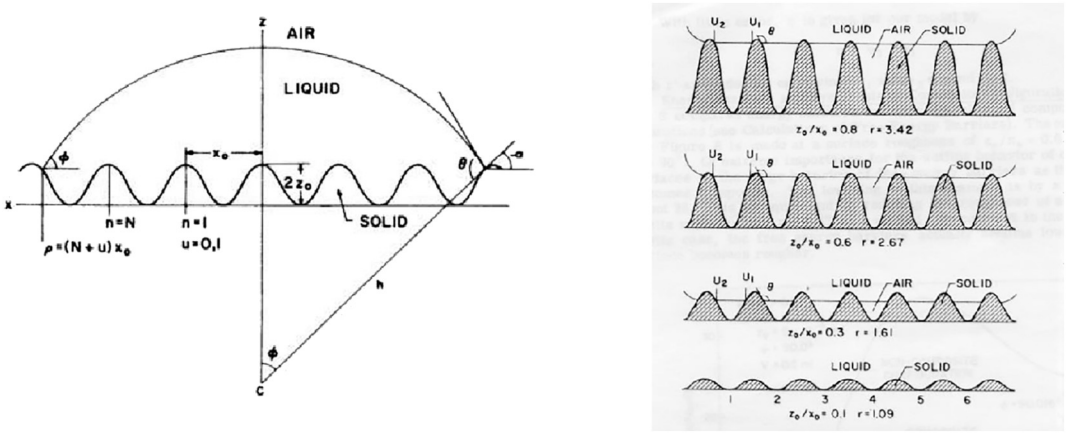

Fig. 1. Geometrical argument by Johnson and Dettre illustrating the role of the local contact angle θ in the Wenzel - CB transition for a sinusoidal surface. θ must obey Young's equation at every microscopic liquid-solid contact line. For a sufficiently high sinusoidal amplitude (i.e. surface roughness), the spreading of the contact line across the region around the sinusoidal inflection point violates Young's law and is therefore forbidden. The limiting local slope $\tan \alpha = -\partial z/\partial x$ across which the contact line can spread is given by the relation $\theta = 180^\circ - |\alpha|$. Reprinted (adapted) with permission from [24]. Copyright 1963 American Chemical Society.

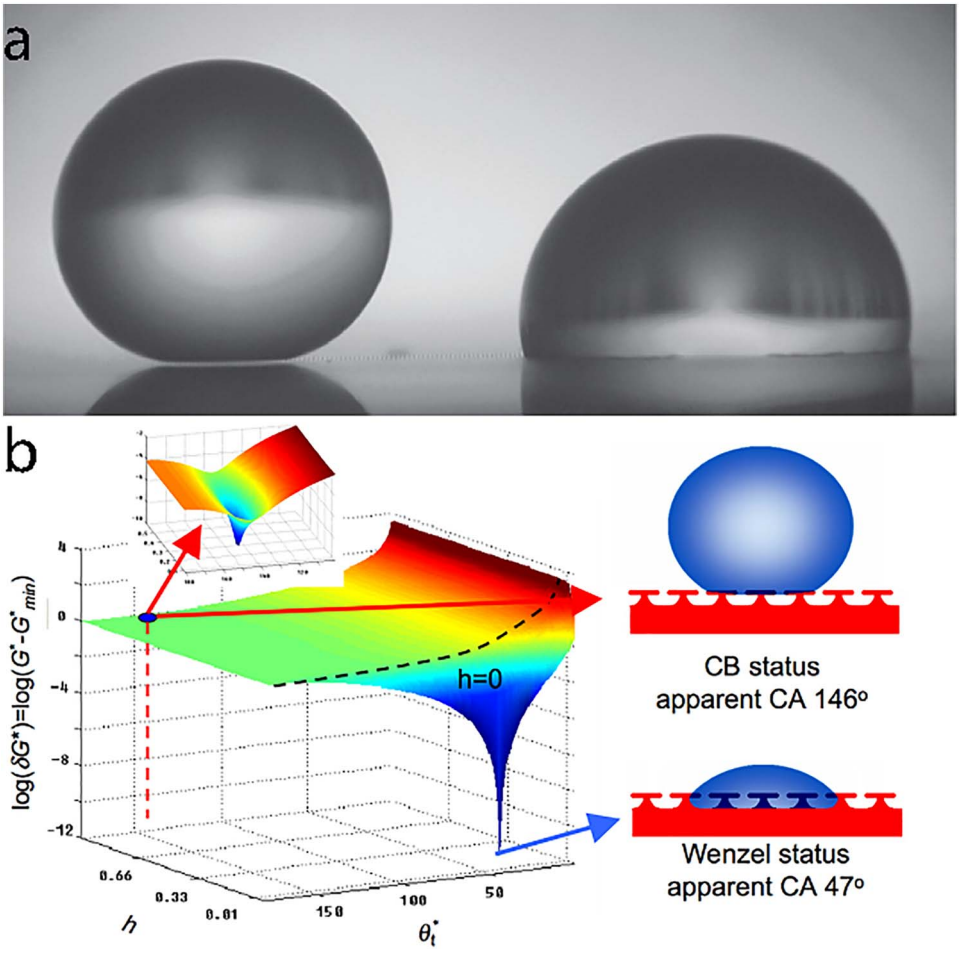

Fig. 2. (a) Coexistence of CB and Wenzel wetting (adapted from [1]). The CB drop was obtained by careful placement on top of the rough surface, while the Wenzel state formed upon impact. Reprinted with permission from Annual Reviews. (b) Landscape in Gibbs free energy density G^* for octane on the structured surface shown on the right, relative to its value of the Wenzel state (G^*_{min}) (adapted from [5]). h is the normalized height of the suspended air-liquid interface with respect to the maximum height of the surface and θ^*_t is the apparent macroscopic contact angle. The inset clearly shows the minimum in free energy of the CB state and the energy barrier between the two wetting states explains why a CB state is readily obtained, despite the lower free energy minimum of Wenzel wetting. Reprinted with permission from AAAS.

the use of external power [39]. More elegantly perhaps, electrocatalytic water splitting using superhydrophobic ZnO nanorods also replenishes the plastron [45], and conical silicon nano-textures exhibit a spontaneous, partial reappearance of the trapped gas phase upon liquid depressurization [46]. Switching between wetting states is easier to perform when a drying phase is included to remove trapped water in the microstructure. In this case, modifying the surface chemistry via acidic and alkaline conditions, or UV light irradiation and thermal heating has been shown as an effective method [47].

Both the kinetic and thermodynamic aspects described here com-

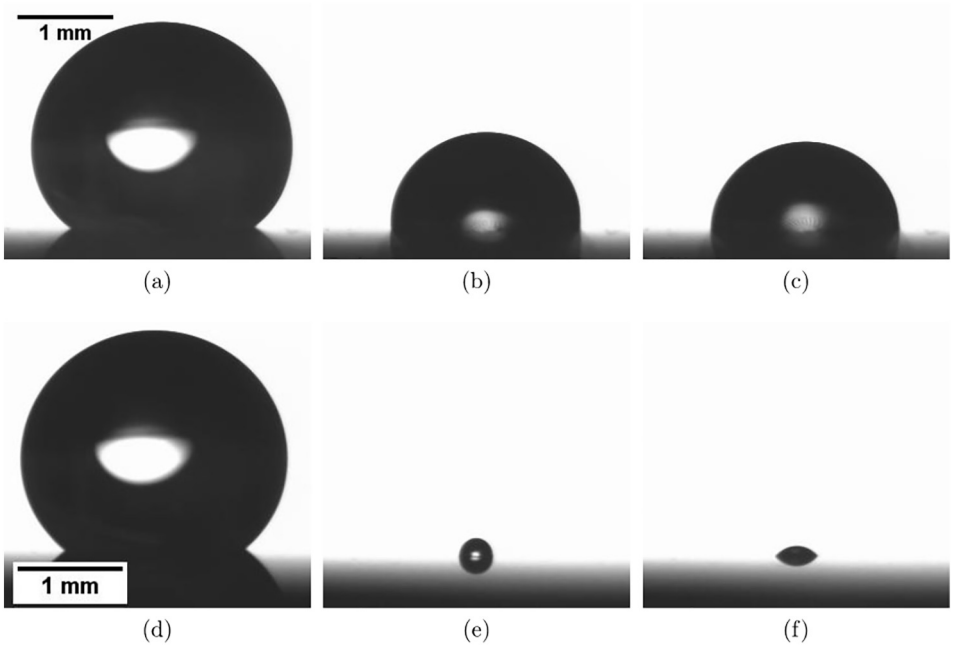

Fig. 3. Transition from the Cassie-Baxter to the Wenzel state by droplet evaporation on two different surfaces, similar to those schematically indicated in Fig. 2(b) (right). Reproduced with permission from [31].

plicate the evaluation of the robustness of superhydrophobicity. Whether superhydrophobic Cassie or pinned Wenzel wetting is obtained does not only depend on the surface itself, by also in the way the liquid is deposited and on other external parameters, such as mechanical motion (e.g. vibration). Furthermore, it is now established that superhydrophobicity of permanently immersed surfaces is thermodynamically unstable and decays through the diffusion of the plastron into water. This rules out the application of superhydrophobicity in vessels or tubes for the storage or transport of liquids. It may also limit some implementation of the drag-reducing effect of superhydrophobicity.

It should be noted that the specific geometry of the surface roughness geometry is an important factor for the thermodynamic stability of the Cassie wetting configuration. It has been demonstrated that hydrophilic materials can possess a Cassie wetting configuration if the water contact line is unable to progress into the gaps of the surface roughness for certain allowed critical contact angle values. This can be achieved using morphologies with air proof structures including honeycomb shapes which can produce a negative Laplace pressure beneath a sessile droplet, and overhanging structures [48–51]. By modifying these geometries accordingly, one can influence the minimum allowed contact angle of a sessile droplet on these surfaces for hydrophilic materials. This in turn has progressed the field's understanding of how to produce thermodynamically and kinetically robust structures for traditional superhydrophobic surfaces using hydrophobic materials.

3. Fabrication methods for robust superhydrophobic surfaces

As discussed in the Introduction, a superhydrophobic surface requires roughness on the micro- and/or nano-scale, in addition to a low surface energy for drops to obtain a Cassie wetting state, where air is trapped in the fine structure of the surface [1,52]. A wide range of methods for the fabrication of superhydrophobic surfaces have been proposed during the past 15 years. However, only recently have a number of publications investigated the robustness of the produced surfaces. The field clearly needs to move beyond the basic proposal of new fabrication methods, and towards a full characterization of robustness and up-scalability if the field is to make technological impact. This Section provides a brief summary regarding different fabrication techniques used over the past 15 years, and will then focus on robustness testing methods.

A common way to categorize fabrication techniques in the literature is to group them as “top down” or “bottom up” approaches [53]. “Top down” refers to the fabrication of a superhydrophobic surface via

Fig. 4. Underwater stability of the plastron on superhydrophobic *Nelumbo nucifera* leaves. Plastron stability was determined by measuring the specular reflection of light of leaves submersed at a depth of 55 cm. Most of the reflectivity decayed within the first hour, but the leaf remained somewhat reflective for up to one week, when it started to decay. This was attributed to the rapid dissolution of the macroscopic plastron, but air remained trapped in the sub-micron surface roughness formed by surface wax crystals. Reproduced with permission from [31].

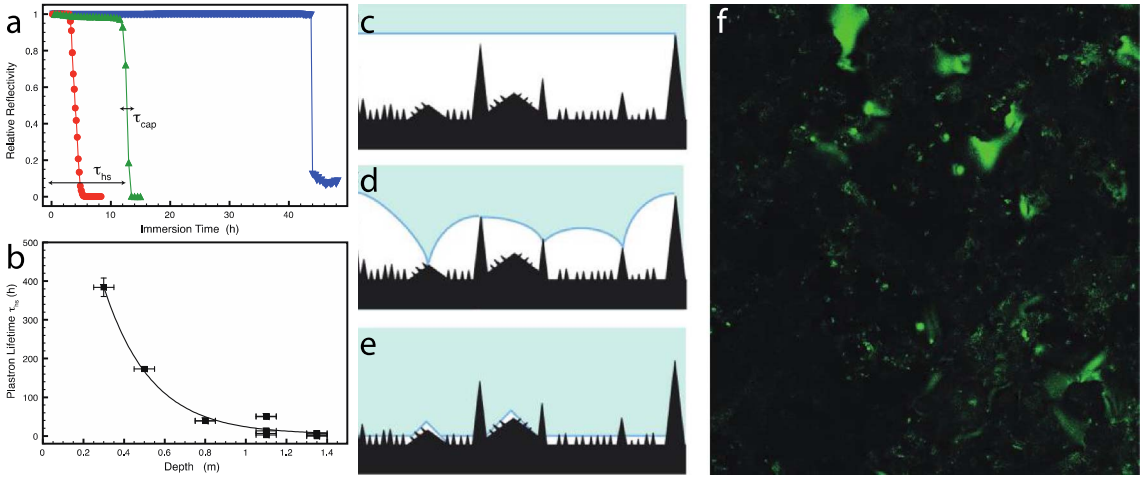

Fig. 5. Underwater plastron stability of a structured Teflon surface, analyzed in a similar way as in Fig. 4. (a) The plastron stability depends strongly on the immersion depth (▼ 0.5 m, ▲ 1.1 m, and ● 1.3 m). The plastron decays in two stages, the thinning of the laterally extended plastron (c), followed by a decay into pinned bubbles (d), which are highly unstable because of the continuously increasing Laplace pressure. This process can be described by an Epstein-Plesset model. The two characteristic decay constants τ_{cap} and τ_{hs} are associated with these two processes. The final state in (e) is characterized by locally trapped air in the sub-micrometer structure of the surface. (f) This process can be followed by confocal microscopy, imaging the plastron and the late-stage bubbles. Reproduced with permission from [13].

roughening by printing, molding, and carving to generate appropriate topographies needed for a superhydrophobic state. In contrast, "bottom up" methods involve the self-assembly of smaller building blocks to form larger, more complex objects. Another way to organize these fabrication techniques is to group them into approaches that render rough materials hydrophobic, and those that create roughness in hydrophobic materials.

There exist many different methods to produce the roughness needed for a Cassie state of drops, mostly resulting in surface topographies both on the nano- and micro-scale. If the roughened material is not sufficiently hydrophobic, further modification by coating them with polymer coatings or self-assembled monolayers (SAMs) is performed to reduce the surface energy. However, this approach incurs a higher risk of losing the superhydrophobic state when these coatings are compromised. While in some techniques the coating adheres well to the substrate, the use of coatings is not always ideal for fabrication of robust superhydrophobic surfaces. Typically, the roughening of an already hydrophobic material, which does not rely on chemical surface modification, is simpler to perform and produces more mechanically and thermodynamically durable superhydrophobic surfaces. These are important qualities when considering large scale/industrial application, as raised by Blossey in 2003 [3].

In terms of fabrication methods, this Section covers a large portion of the approaches that have been used over the past 15 years and comments on their expected durability. Reporting robustness on superhydrophobic surfaces has not been common practice until the past 5 years, and it still suffers from a lack of standardized testing methods, often making comparisons difficult [54]. Thus, a large number of different papers published in the field do not present data on their surface robustness, particularly early papers which pioneer fabrication methods. To provide context regarding the field and development of superhydrophobic surfaces, several examples are expanded in more detail corresponding to publications that are among the most highly cited in the field. Here we focus on solid/air interfaces (lotus leaf mimics), as opposed to liquid impregnated surface (pitcher plant mimics), which will be touched upon later.

4. Robustness of surfaces produced with established fabrication methods

4.1. Lithography and templating

Lithography involves the controlled patterning of surfaces, whereby large or micro-/nano-scale morphologies are transferred from a hard or soft master to the desired substrate. This can be achieved by imprinting, depositing or etching around a pre-designed pattern. These methods can further be subdivided into a variety of different approaches depending on desired materials and morphologies, which include X-ray lithography [55], electron beam lithography [56,57], photolithography [58–61], micro-contact printing [62–65], colloidal lithography [66], and nano-imprint lithography [67–70].

Following the investigation into nano-patterning via capillary forces by Suh et al. [71], Jeong et al. used imprinting of lithographic patterns to produce micro- and nano-scaled patterns of polystyrene (PS) and poly(methyl methacrylate) (PMMA), spin coated onto on silicon substrates [72]. A polydimethylsiloxane (PDMS) mold possessing a micro-sized topography was imprinted above the coated polymer's glass transition temperature T_g. This process was repeated with a poly (urethane acrylate) (PUA) mold with nano-sized features on the micro-patterned surface to produce a hierarchical surface. The resultant multi-scale superhydrophobic surface displayed a static contact angle of 161° and easy droplet roll off (Fig. 6). This technique results in potentially robust surfaces limited by the mechanical properties of the high-T_g polymer. Additionally, this technique leaves room for use of other polymers for different application needs.

Sacrificial templating is a technique which makes use of lithographic processes by replicating desired surface features by pressing/molding a soft/flowing polymer over the desired surface morphology. After the polymer has hardened, the template (commercial inorganic membranes, masters prepared by lithographic process and natural lotus leaves) [14,61,65–68,73–76] can be dissolved away, leaving behind the patterned material.

After Autumn et al. developed an approach that mimics gecko adhesive foot-hair [77], Jin et al. used the same templating method to fabricate a layer of polystyrene (PS) nano-tubes, in an attempt to imitate the unique structure of the fine hairs (Fig. 7) [78]. Commercially available nanoporous alumina membranes were coated with a thin PS layer, and the template was dissolved away by a basic solution at room temperature, resulting in a superhydrophobic surface with a static contact angle of 162°, and a complete adhesion of the droplet on the pillars. This apolar structured surface made from a hard plastic should possess some degree of robustness but the high aspect ratio fibers are probably not very stable under shear.

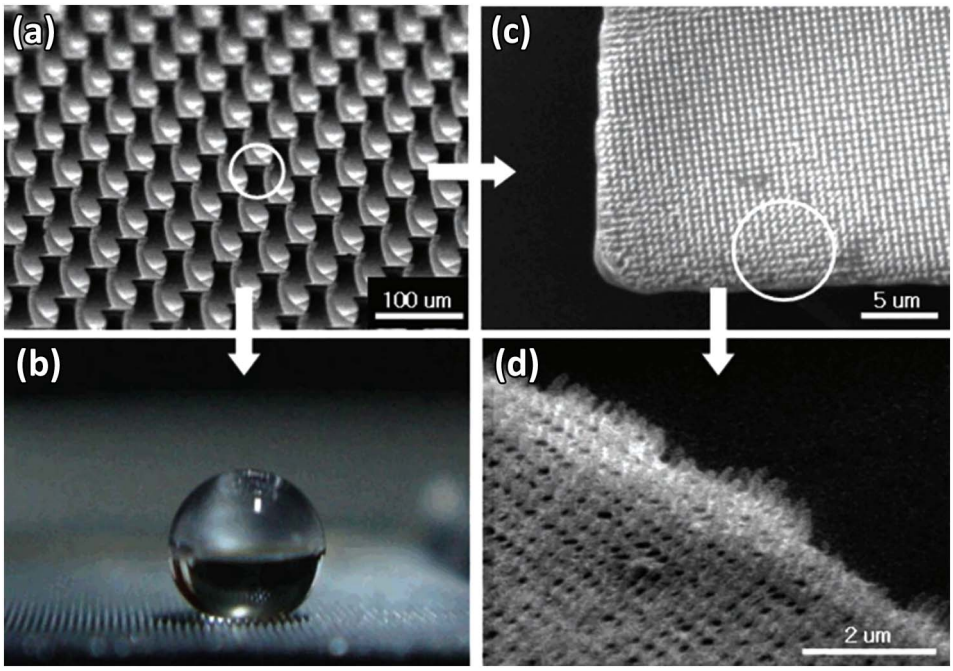

Fig. 6. Hierarchical micro-/nano-scale PMMA structures: (a) micro-posts, with diameter, height and spacing of 30 μm, 50 μm, and 40 μm respectively. (b) water droplet in contact with this surface, (c), nano-pillars, with diameter, height and spacing of 100 nm, 450 nm and 400 nm respectively (d) magnification of (c). Reprinted (adapted) with permission from [72]. Copyright 2006 American Chemical Society.

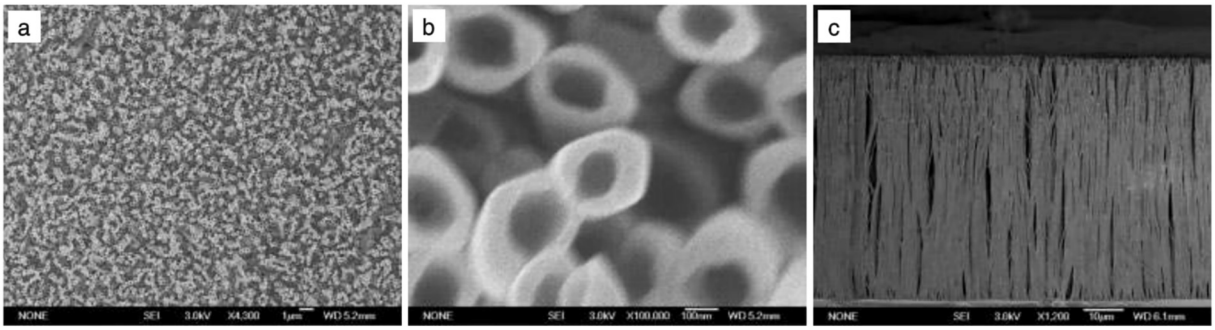

Fig. 7. (a) Top view of polystyrene nano-tube layer. (b) Magnification of (a). (c) Cross-sectional view of polystyrene nano-tube layer. Reproduced by permission from [78]. Copyright 2005 John Wiley & Sons.

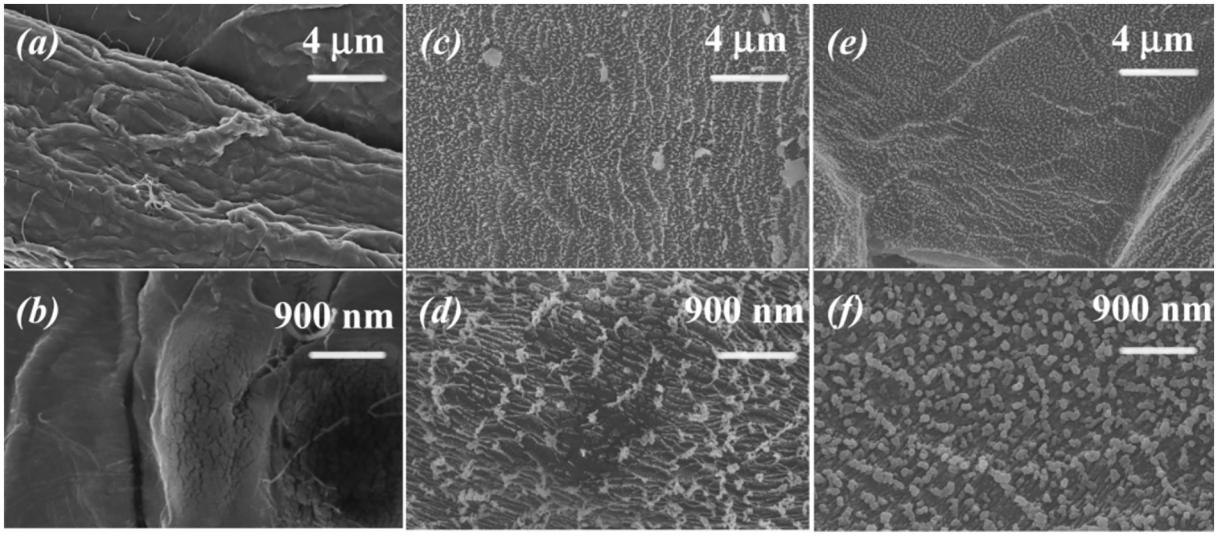

Fig. 8. (a)–(b) The surface of paper before and, (c)–(d) after oxygen-plasma etching, and (e)–(f) after PFE coating (tetrafluoroethene). Reproduced (adapted) with permission from [93]. Copyright 2008 American Chemical Society.

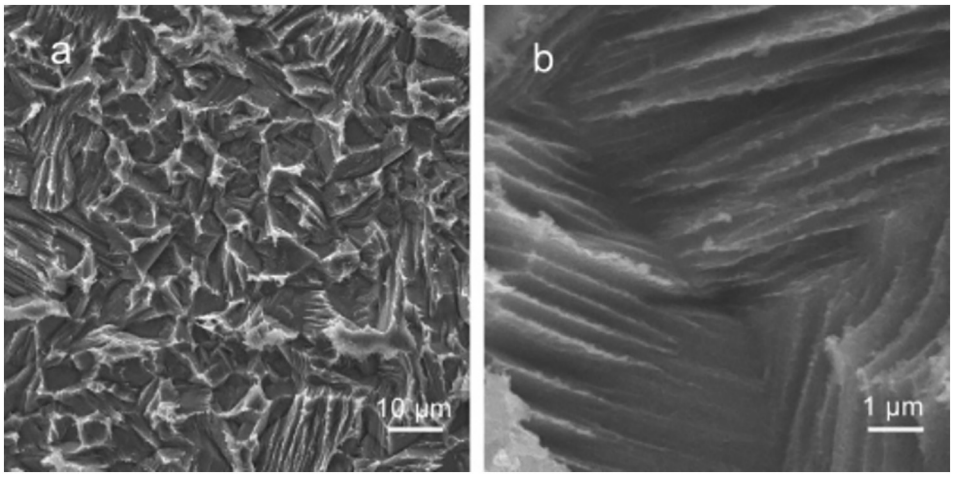

Fig. 9. Roughened zinc surface etched with a 4.0 mol L^{-1} HCl solution for 90 s at room temperature. Reproduced (adapted) with permission from [95]. Copyright 2005 American Chemical Society.

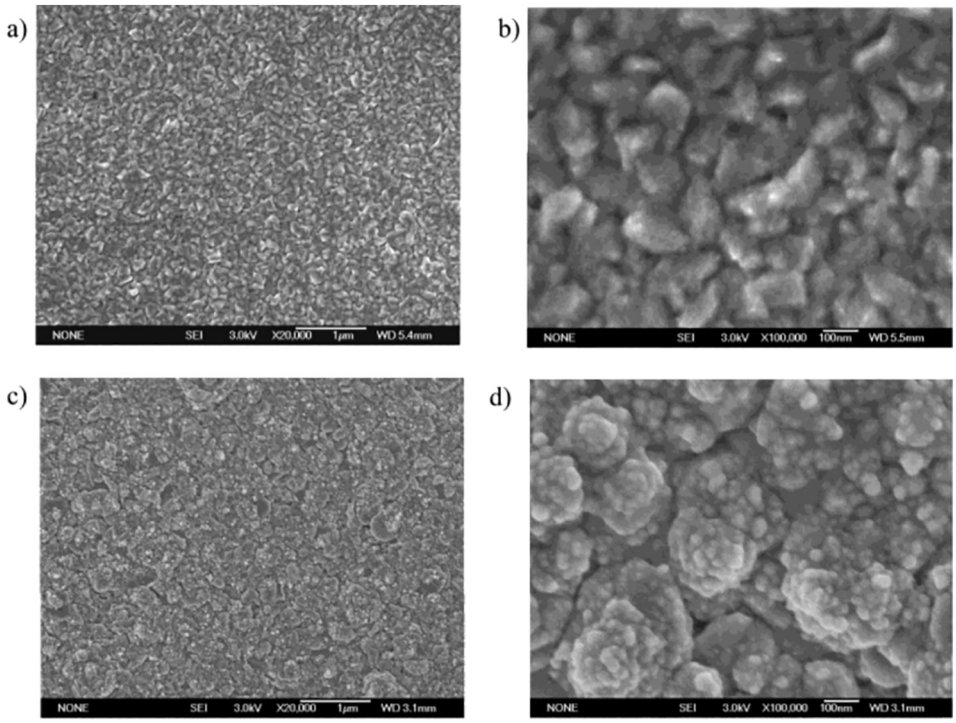

Fig. 10. (a)–(b) ZnO film catalyzed by Ni; (c)–(d) A superhydrophobic ZnO film, catalyzed by Au, showing a hierarchical structure. Reproduced (adapted) with permission from [98]. Copyright 2004 American Chemical Society.

4.2. Plasma and chemical etching

Plasma and chemical etching are both methods used to induce random roughness in a surface. These techniques can be used as the primary method of surface roughening, or in combination with other techniques, such as lithography, to add additional micro- and nano-scale roughness. Plasma etching is performed via the bombardment of a surface with reactive atoms or ions that are generated in a gas discharge. This technique is capable of creating defined topographical features including deep grooves with steep walls [75,79–92].

Balu et al. produced nano-scale roughness on cellulose paper using domain selective etching of amorphous cellulose portions in an oxygen plasma (Fig. 8) [93]. A thin fluorocarbon film was subsequently deposited via plasma-enhanced chemical vapor deposition, producing superhydrophobicity with low roll off and a static contact angle of 166°. As this surface is essentially chemically coated paper, its use is limited to specific applications. However, it is very versatile due to its simple and accessible materials. Mechanical robustness is probably a minor criterion in this approach, due to the disposable nature of the product.

Chemical etching generates surface roughness by immersing the target surface in a corrosive/reactive chemical mixture [94–97]. This treatment is commonly used on metal and glass surfaces.

Qian and Shen performed simple chemical etching of polycrystalline aluminium, copper and zinc to produce micro- and nano-scale roughness [95]. After chemical etching via immersion in specific corrosive solutions, a fluoroalkylsilane coating was applied to produce the required hydrophobic surface energy. A zinc superhydrophobic surface was produced by etching with concentrated HCl for 90 s prior to coating (Fig. 9). The coated surface exhibited superhydrophobicity with static contact angles of about 155° and roll-off angles of approx. 6°. The surface itself is likely to have strong mechanical robustness, but it is defect prone when the coating is damaged and its long-term perfor-

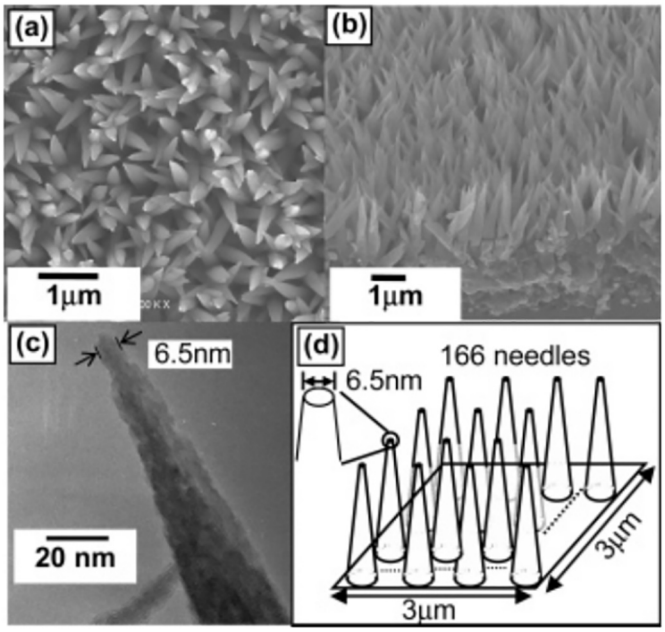

Fig. 11. (a), (b) and (c) Brucite-type cobalt hydroxide films; (d) schematic of the film. Reproduced (adapted) with permission from [103]. Copyright 2005 American Chemical Society.

mance is limited by the degradation of the fluorinated layer.

4.3. Chemical deposition

In chemical deposition, a deposit forms via a surface chemical reaction, forming a layer with a nano-scale topography including nano-pins and nano-rods. A variety of the methods can be used, including chemical vapor deposition (CVD), which utilizes a gaseous precursor to deposit particles or films, chemical bath deposition (CBD) and electrochemical deposition (ECD), which use wet chemical solutions or electrochemically conductive substrates to deposit solid metals and oxides [98–106].

Following work published on ZnO nano-rods with switchable wettability [107], Liu et al. fabricated a superhydrophobic ZnO sub-micrometer thick film via Au-catalyzed chemical vapor deposition (Fig. 10) [98]. This technique produced a surface with hierarchical morphology comprising of nano-structures on sub-microstructures, with a static water contact angle of 164°. Switchable wettability of the resulting superhydrophilic surface was obtained by UV illumination, and superhydrophobic properties could be recovered by placing it in the dark or by heating. This work does not report contact angle hysteresis. Further surface treatment with a stable hydrophobic coating would increase the thermodynamic robustness of this surface.

Hosono et al. used CBD to obtain an array of metal hydroxide nano-needles (Fig. 11) [103]. A solution of $CoCl_2$,$6H_2O$ and NH_2CO in water was used to deposit single crystalline pins of brucite-type cobalt hydroxide on glass slides via immersion. After physisorption of lauric acid to modify the surface energy, they obtained a superhydrophobic surface with a water CA of 178°, with the CA hysteresis not characterized. Since this surface relies on a physisorbed chemical coating to obtain its low surface energy, its superhydrophobicity may be compromised by exposure to environmental conditions. The base material being comprised of a rigid material may result in some degree of mechanical robustness, but the thin needle-like structure quality is probably weak under shear and mechanically induced defects in the organic coating may limit its defect tolerance.

4.4. Colloidal assembly and layer by layer deposition

Colloidal assembly involves the spontaneous assembly of closely packed arrays of colloidal particles, either polymeric or inorganic, on a surface through chemisorption or physisorption [108,109]. Varying the size of assembling particles can result in multi-layered roughness [110], and several combinations of approaches have achieved the hierarchical structures required for superhydrophobic surfaces [111–123].

Zhang et al. used colloidal assembly to produce an irregular binary structure with hierarchical roughness [121], extending earlier work by Velikov et al. [124]. $CaCO_3$-loaded hydrogel spheres approx. 790 nm in

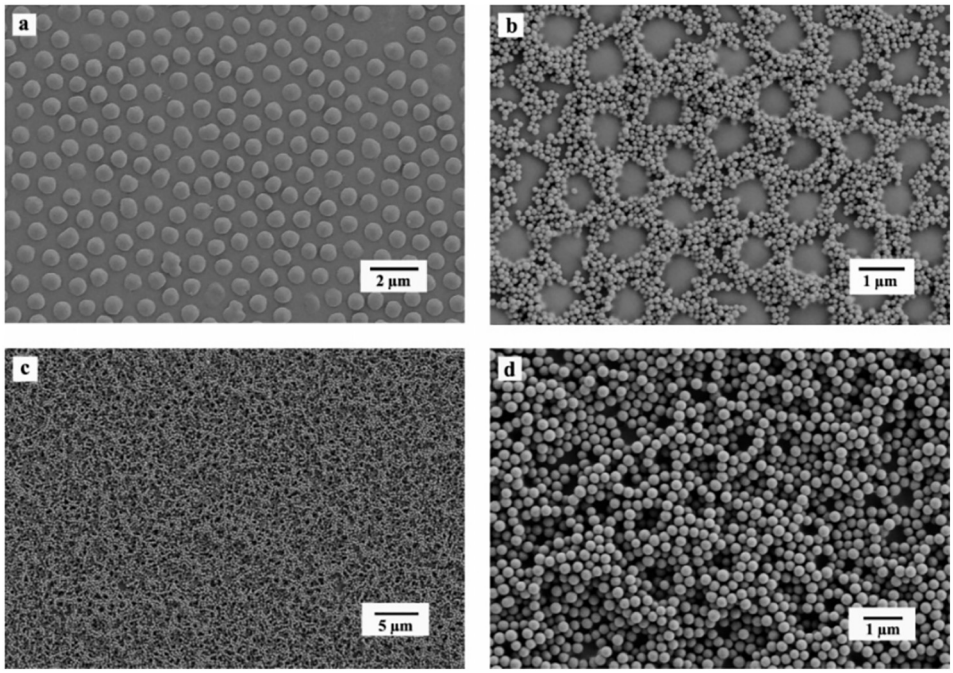

Fig. 12. (a) Array of $CaCO_3$-PNIPAM particles produced by dip-coating of a silicon water into an aqueous particle dispersion. (b) Binary colloidal assemblies produced by dip-coating the sample in (a) into an aqueous dispersion of 296 nm silica spheres. (c)–(d) Binary colloidal assemblies made using a more concentrated aqueous dispersion of 296 nm silica spheres. Reproduced (adapted) with permission from [121]. Copyright 2005 American Chemical Society.

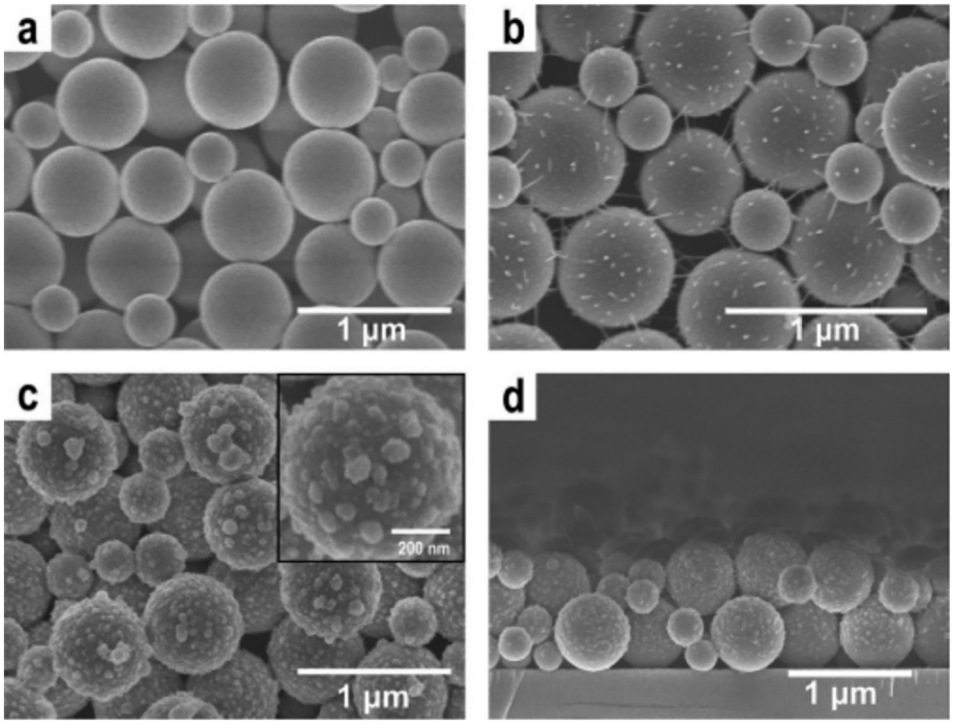

Fig. 13. (a) Surface deposited silica spheres (b) Cross-linked with SiCl4; (c) Coated with 5 PDDA/sodium silicate multilayers via LBL deposition; (c). Inset: Magnification of (c). (d) Cross-sectional view of the silica sphere coating. Reproduced (adapted) with permission from [131]. Copyright 2007 American Chemical Society.

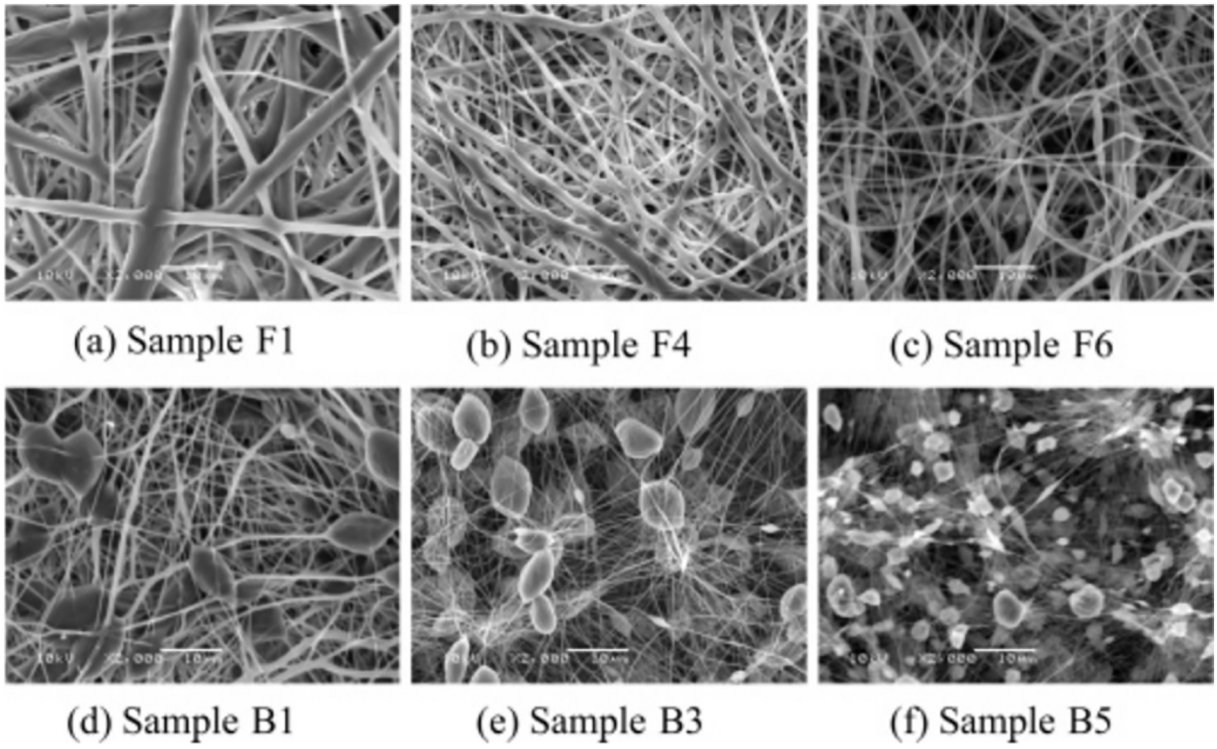

Fig. 14. Polycaprolactone electrospun mats. (a)–(c) Fibrous morphology; (d)–(f) Addition of beaded features. Scale bars = 10 μm. Reproduced (adapted) with permission from [137]. Copyright 2005 American Chemical Society.

diameter were deposited onto silicon wafers by dip-coating, serving as a template for the self-assembly of 300 nm silica or polystyrene particles applied in a second dip-coating (Fig. 12). Superhydrophobicity was achieved through the subsequent application of a self-assembled monolayer (SAM) of hexadecanethiol (HDT) after sputter coating of 30 nm of gold. Mechanical stability was said to be improved by annealing at 500 °C for 2 h, but no testing resulted were presented. The contact angle hysteresis was also not reported, nor the surfaces stability upon immersion in a solvent. Apart from structural limitations regarding robustness, the gold-thiol bond is not thermodynamically stable upon exposure to UV radiation and oxygen, resulting in degradation and subsequent loss of surface qualities [125,126]. This

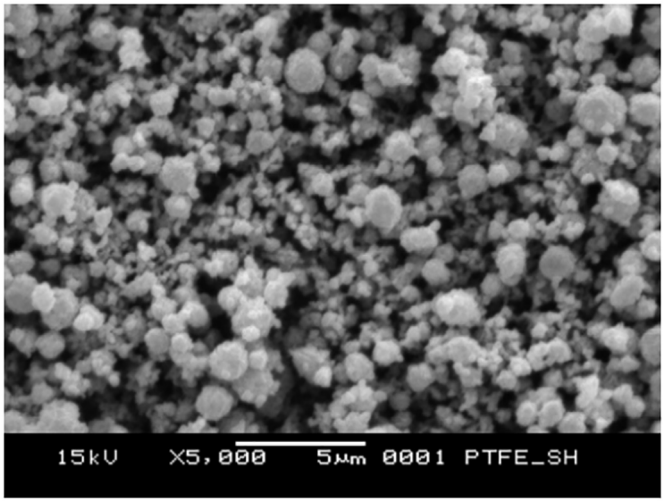

Fig. 15. Electrosprayed PTFE with 20 min deposition time. Reprinted from [145], Copyright 2007, with permission from Elsevier.

reduces the overall robustness of the surface significantly, not taking into consideration the mechanical properties of this surface which may be limited by the weak colloidal interactions.

In addition to immersion and spin-coating, layer by layer deposition (LBL) has been used to apply multi-layer films on desired substrates, by using the electrostatic attraction of colloids and polymers with the alternating surface charge [113,127–130]. The layers are often combined with colloidal particles to further increase the surface roughness.

Utilizing sub-micron silica spheres, Zhang et al. used the deposition of poly(diallyldimethyl-ammonium chloride) (PDDA)/sodium silicate multi-layer films on a silica-sphere-coated substrate to produce hierarchical roughness (Fig. 13) [131]. Superhydrophobicity was achieved by applying a layer of fluoroalkylsilane by chemical vapor deposition, resulting in a static water contact angle of 157° and low sliding angle. The robustness of these surfaces was not reported, but based on the physically absorbed multilayers for roughness, and the surface dependence on a self-assembled monolayer, the overall chemical and mechanical robustness is probably limited. This surface could be improved by using hydrophobic materials for the generation of roughness, and by chemical bonding of the applied layers to the substrate.

4.5. Electrospinning and electrospraying

In electrospinning, an electrical potential is applied between an extrusion nozzle and a grounded collection plate; as the polymer is ejected, the solvent rapidly evaporates, resulting in the formation of a mat of fibers on a collection plate. These fibrous morphologies can be further chemically modified and can incorporate solvents in their porous structure [132–137].

Following previous work on electrospinning [132], Ma et al. combined electrospinning and CVD to produce superhydrophobic surfaces for use on fabric [137]. Polycaprolactone (PCL) mats were produced with fibrous morphologies via electrospinning, controlling the formation of additional beaded features (Fig. 14). Further coating with perfluoroalkyl ethyl methacrylate (PPFEMA) achieved the desired low surface energy, producing static contact angles of 175°, allowing the water to roll off freely. The robustness of these surfaces was not reported. Based on the materials used for fabrication and the fibrous network morphology, some degree of mechanical toughness can be expected, in addition to the versatility of use as a fabric. The performance of this material is probably limited by the stability of the physisorbed layer, which is required to achieve superhydrophobicity.

Electrospraying is better suited for the deposition of beads rather than fibers [138]. In electrospraying, the polymer solution is dispensed from a capillary nozzle maintained at a high potential onto a desired substrate, whereby the electric field forces the ejected polymer into fine droplets [16,139–144].

Burkarter et al. produced micro- and nano-scale rough superhydrophobic surfaces by depositing a commercial suspension of polytetrafluoroethylene (PTFE) in water on fluorine doped tin oxide (FTO)

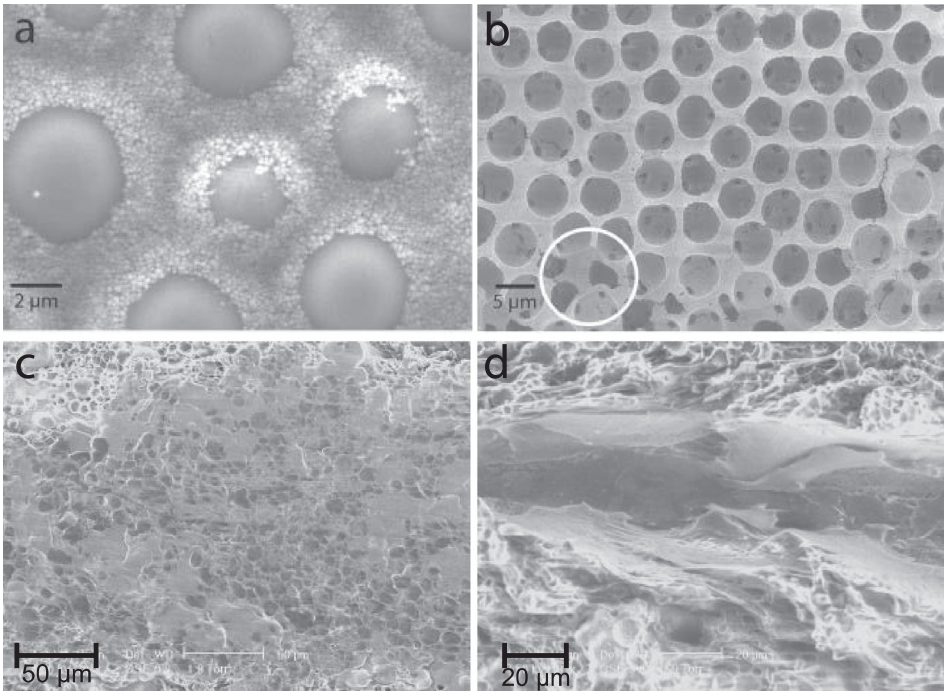

Fig. 16. (a) The co-deposition of larger polystyrene spheres with small PTFE colloids, which (b) results in the porous surface with a water contact angle of ~170° and a negligible contact angle hysteresis. (c) Mechanical testing by translating a parabolic tip under load retains some of the surface roughness for pressures up to 120 MPa; (d) however, mechanical testing at 290 MPa causes the delamination of the PTFE film from its support. Reproduced with permission from [148].

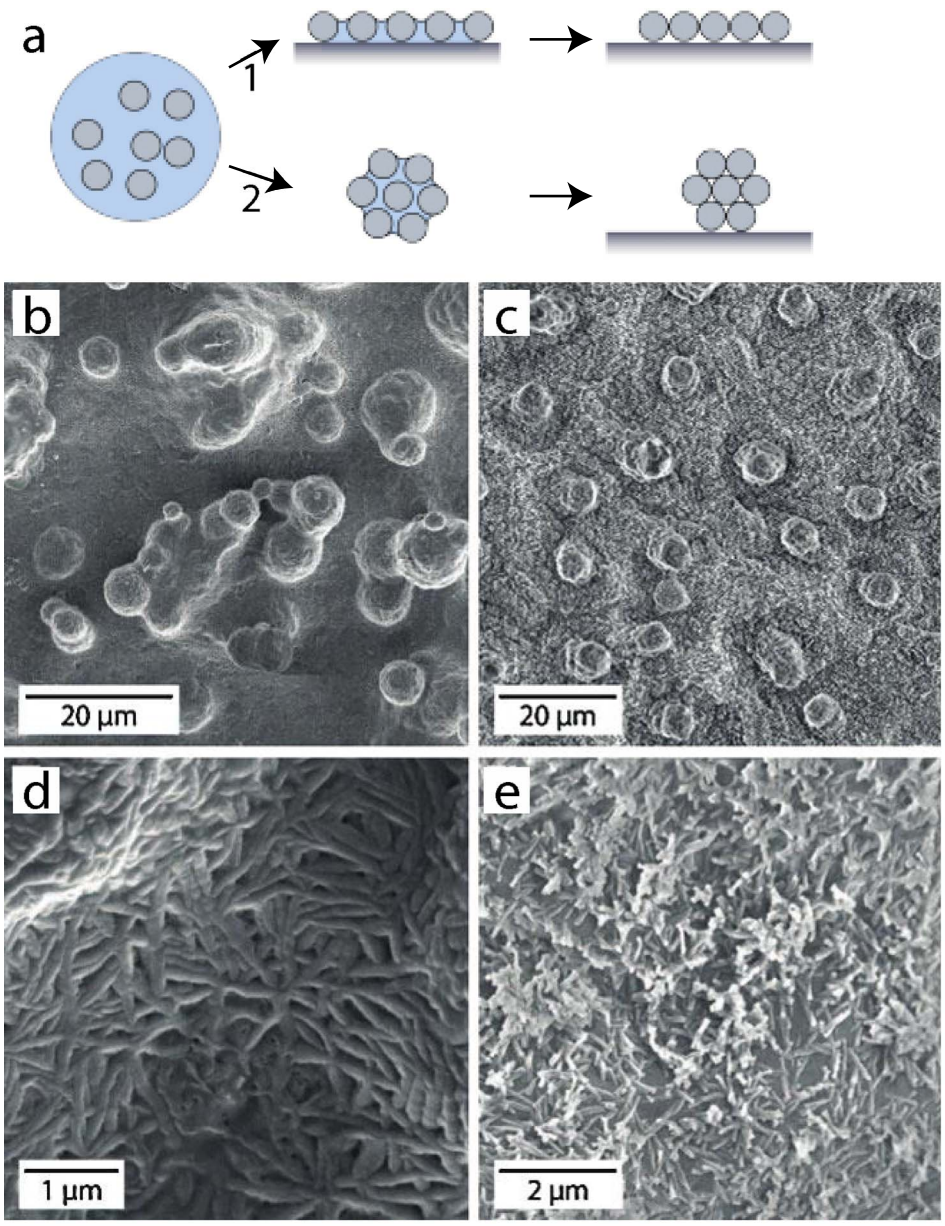

Fig. 17. (a) Schematic of PTFE film formation. In the standard route 1, the suspension wets the surface. Capillary forces during the subsequent drying pull the colloidal spheres together, thus aiding the film formation. In approach 2, this occurs during the flight phase of the suspension drop, causing the formation of a dry cluster that deposits onto the surface. The obtained result in (b,d) is very similar to that of a lotus leaf (c,e), both in terms of its micro- (b,c) and nano- (d,e) texture. Reproduced with permission from [13].

coated glass slides by the electrospray technique (Fig. 15) [145]. The resulting surface morphology had a static contact angle as high as 167° with drop sliding angles of 2°. The authors note that this surface fails under wear and abrasion, which would need to be improved by increasing the adhesion between the particles and the substrate.

4.6. Teflon-derived surfaces

Polytetrafluoroethylene (PTFE) is the traditional and still one of the most wide-spread materials for the manufacture of non-stick surface coatings. Its very low surface energy and wide availability therefore make it interesting for the manufacture of superhydrophobic surfaces, which to some extent is offset by the difficulty in processing many fluoropolymers and by their cost. Since PTFE coatings are typically made by depositing a colloidal suspension, followed by high-temperature sintering, it is convenient to modify the established coating protocols in such a way that produces PTFE surfaces that are sufficiently rough to be superhydrophobic. A facile way to achieve this is to blend the PTFE suspension with a second colloidal suspension of lower thermal stability, such as polystyrene, or polymethyl methacrylate [146]. For the case where the latter spheres are much larger than the PTFE colloids, an inverse opal PTFE structure is formed that has superhydrophobic properties (Fig. 16). The tuning of pore sizes and densities yield surfaces with static water contact angles of ~170 °C, and negligible contact angle hysteresis. In an alternative approach, embedded salt crystals were used, replacing the sacrificial polymer spheres [147].

The mechanical robustness of these layers was tested by laterally translating a parabolic stainless steel point across the sample under varying normal pressures [148]. While the samples suffered only from minor structural damage for pressures up to 120 MPa, the film failed by delamination from the substrate at higher pressures (Fig. 16). The surface remained superhydrophobic for pressures below 1 MPa. While water drops on samples that were rubbed with pressures above 1 MPa were in the Wenzel state with higher contact angle hysteresis, their wetting performance both in terms of static contact angle and contact

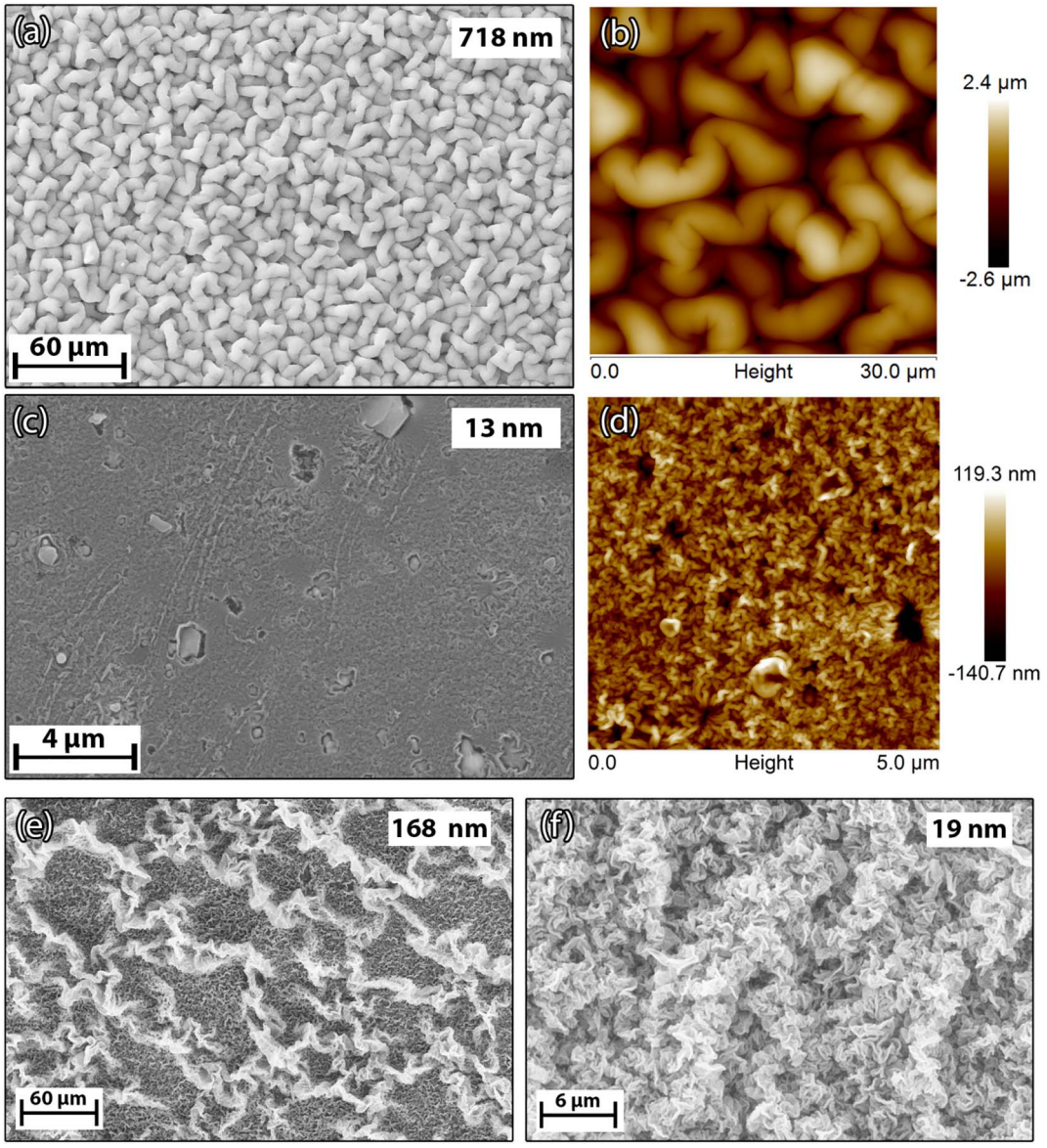

Fig. 18. (a)–(d) Selection of SEM micrographs with corresponding AFM images of induced wrinkle topographies arising from the annealing of Polyshrink™ coated with varying Teflon AF layer thicknesses, indicated in each picture. (e) and (f) SEM micrographs of induced wrinkle topography arising from annealing of polyolefin sheets coated with varying Teflon AF layer thickness, indicated in each image. Reproduced (adapted) with permission from [188]. Copyright 2016 American Chemical Society.

angle hysteresis remained superior to that of the surfaces achieved with the standard wetting protocols [148].

A second approach also using PTFE is a slight modification of the industrially used spray coating techniques [13]. In its standard implementation, the sprayed-on film forms a homogeneous layer, which compacts during the evaporation of the liquid phase (typically water). This process is largely driven by capillary forces that aid the dense packing of the colloidal spheres during drying. The resulting dense colloidal packing aids the film formation during the sintering step, yielding a high-density layer of high mechanical toughness. Fig. 17 shows an alternative deposition strategy. By increasing the flight time of the spray, water evaporates from the suspension droplets, forming dry solid aggregates. The deposition of these aggregates onto a pre-formed homogeneous PTFE surface induces a roughness that is retained upon high temperature sintering. The resulting surface closely resembles the structure of a lotus leaf, as shown in Fig. 17. While these superhydrophobic surfaces were not systematically tested they have a mechanical robustness that is comparable to the ones in Fig. 16. A recent method for creating the roughness required for superhydrophobicity was performed by simply roughening PTFE with different grades of sandpaper [149], which presents a simple alternative to the above mentioned techniques.

4.7. Other techniques

The techniques mentioned above cover the most common methods for producing surface roughness, however there are other chemically more complex approaches that we have not covered. These include: sol-gel techniques that can be used for depositing porous structures on glass [150–156]; phase separation [157–162]; and block copolymers micelles [163,164].

5. Robustness of surfaces produced with emerging fabrication techniques

In recent years, the focus has shifted towards industrial applications and towards multi-functionality in the fabricated surfaces, including reflection and transparency [116,151,165–170], switchability [141,171–175], and self-healing properties [16,176–181]. The following are examples of more recent techniques for fabrication of super-

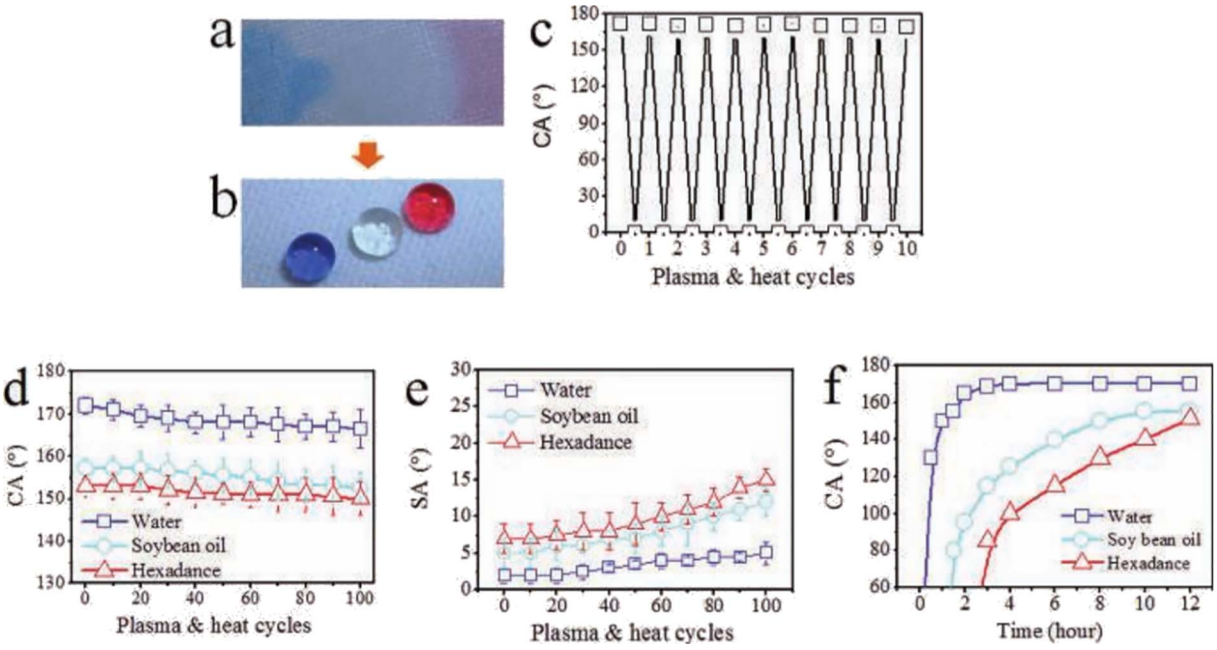

Fig. 19. Droplets of water (blue), hexadecane (red) and soybean oil (transparent) spread on (a) a coated fabric after the first plasma treatment; (b) dewet into spherical shapes on the coated fabric after 100 cycles of plasma and heat treatment. (c) Water contact angle values during the first 10 cycles of treatment. (d) Contact angle and (e) SA (sliding angle) versus number of treatment cycles. (f) CA of the indicated solvents change with ageing time at room temperature (after 100 cycles of plasma-and-heat treatment). Reproduced (adapted) from [15]. Copyright 2013 John Wiley & Sons. (For interpretation of the references to color in this figure legend, the reader is referred to the web version of this article.)

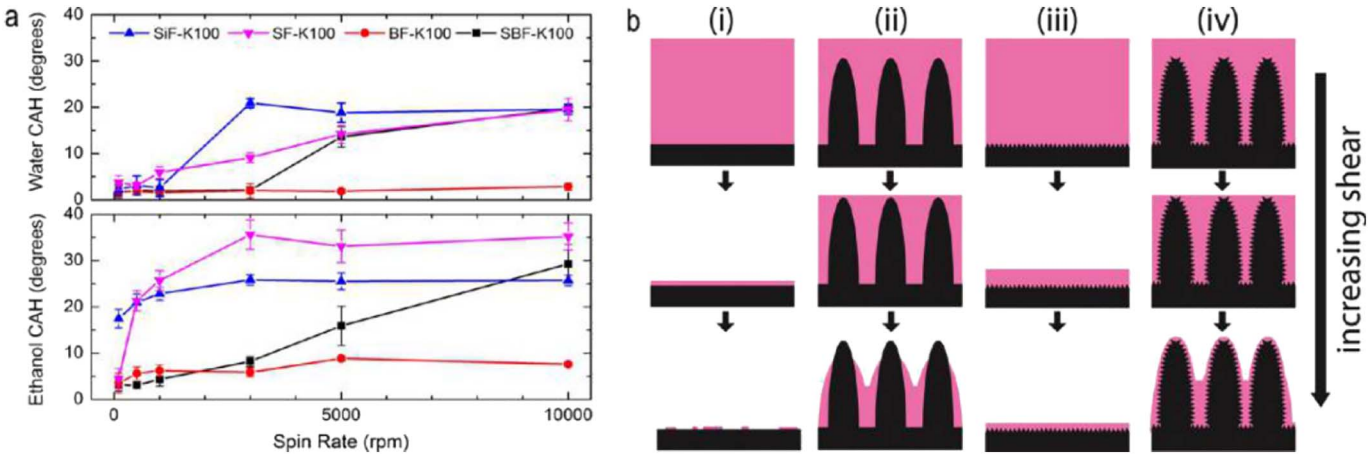

Fig. 20. (a) Contact angle hysteresis of water (top) and ethanol (bottom) on four different lubricated substrates after spinning for 1 min at the shown spin rates. (b) Evolution of the lubricant layer with increasing shear on the (i) flat fluorinated silicon wafer (SiF), (ii) micro-scale textured surface (SF), (iii) a hierarchically textured surface (SBF), and (iv) uniformly nano-textured surface (BF). All samples were lubricated with excess amount of perfluoropolyether lubricant. Reproduced (adapted) with permission from [201]. Copyright 2013 American Chemical Society.

hydrophobicity, addressing robustness and up-scalability.

5.1. Wrinkling

A simple method for generation of surface roughness is the wrinkling of a rigid film on a shrinkable substrate [182–185]. Wrinkling can occur for example by the contraction of a bulk phase covered by a rigid thin film, resulting in the buckling deformation of the surface layer (wrinkles and folds which may further distort into creases, or, in extreme cases lead to the delamination of the films). This process is an effective and spontaneous approach to producing the surface roughness needed for superhydrophobicity. Fu et al. in 2009 deposited thin layers of gold (15 nm) via sputter coating onto sheets of extruded polystyrene, Polyshrink™, which was subsequently annealed at 160 °C [186]. To produce effective superhydrophobic surfaces, hard polymers can be used as the rigid top layer, which has been demonstrated by Manna et al. in 2013 [187], who used a hydrophobic polymer multilayer as the rigid top layer. This simple approach to generate complex surface roughness with a minimal effort was applied onto 'shrink wrap' as the substrate.

Scarratt et al. demonstrated a simple two-step process for the fabrication of a superhydrophobic surface by wrinkling a uniform layer of a Teflon Amorphous Fluoropolymer (AF) on sheets of extruded polystyrene and polyolefin [188]. Upon annealing for 2 min at 160 °C the sheets shrunk by 70% and 90% of their original size, respectively. The resulting single scale and hierarchical wrinkle morphologies obtained are shown in Fig. 18.

The double scale hierarchy wrinkled surfaces produced on a polyolefin substrate showed static water contact angles of 175°, with roll off angles < 5°. Using shrink wrap as a substrate shows great potential for wrapping 3D objects during the annealing phase. The mechanical robustness was tested by cavitation, nano-scratch and nano-

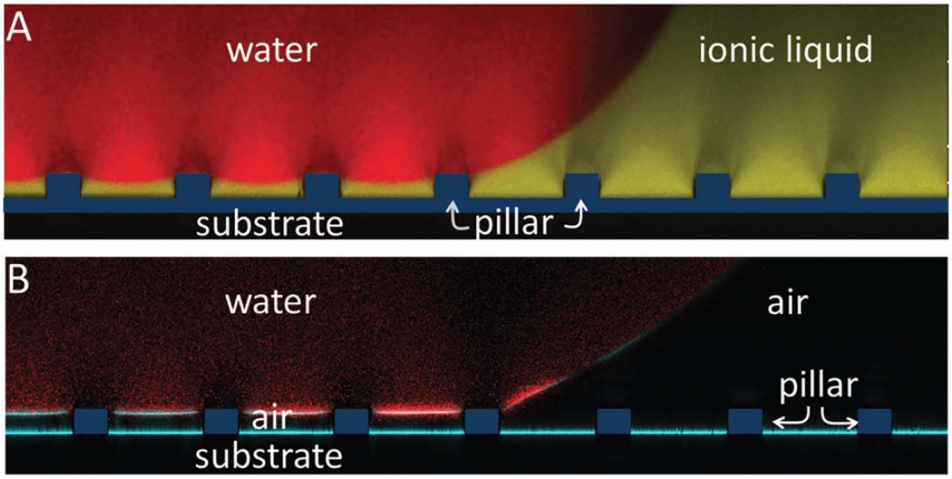

Fig. 21. A water droplet (red) deposited on (a) an ionic liquid (yellow) infused into a micro-pillar array (dark blue); the drop rests on the pillars' tops, with the space between the micro-pillars filled with lubricant; and on (b) a superhydrophobic surface. Pillar distance 40 μm, diameter 10 μm, and height 10 μm. Reproduced with permission from [198]. Published by the Royal Society of Chemistry 2015. (For interpretation of the references to color in this figure legend, the reader is referred to the web version of this article.)

indentation, which revealed that they have durable mechanical properties, and have the potential for industrial applications, comparing well against commercial optical lens and aluminium film coatings.

5.2. Self-healing superhydrophobic surfaces

As a means to improve the longevity of superhydrophobic surfaces, self-healing properties have been pursued in recent literature [16,17,19,178,189]. These present a promising potential for industrial application, with the ability to recover the surface's superhydrophobic properties after damage. Self-healing mechanisms vary depending on the materials used, and revolve around exposing the surface to a particular stimulus, i.e. light and/or heat treatment to trigger the regenerative process.

Zhou et al. produced a self-healing superamphiphobic surface by coating a fabric with poly(vinylidene fluoride-*co*-hexafluoropropylene), fluoroalkyl silane, and modified silica nanoparticles [15]. The resistance to abrasion of their material was tested by exposing it to laundry and abrasion cycles which did not significantly affect its wettability. Following chemical robustness tests, using strong acid, base, ozone, and boiling treatments, their surface recovered its original properties upon heating over a short time, or ageing at room temperature (Fig. 19). The mechanism behind the self-healing properties of this material is suspected to be due to molecular migration of the fluorinated alkyl chains towards the surface, driven by a need to reduce the free energy after to exposure to polar surface groups generated via chemical abrasion.

5.3. Slippery liquid-infused porous surfaces (SLIPS)

As opposed to the lotus leaf which traps air in the micro- and nano-structure, imitating the liquid infused surface of the pitcher plant shows a great deal of promise in developing robust liquid repellent surfaces [190–199]. A surface with a micro- and nano-structure is impregnated with a liquid, which is immiscible with the liquid to be repelled. This impregnated liquid replaces the air in the Cassie model, thereby creating a surface on which the contacting liquid cannot progress into a Wenzel wetting state. The fabrication of stable SLIPS usually entails nano- and/or micro-scale roughness immobilizing the lubricant layer via capillary wetting. The retention of the lubricant is dependent on its chemical affinity with the substrate in air, and when in contact with or submerged in the liquid to be repelled.

Epstein et al. produced a surface with superior anti-fouling properties through infusing perfluoropolyether into a porous polytetrafluoroethylene (PTFE) substrate or into a microstructured fluoro-silanized Si wafer [200]. This work highlights the principle that any rough surface fabrication technique capable of producing superhydrophobicity can be applied to SLIPS with the appropriate surface chemistry and lubricant combination. They tested lubricant infused surfaces with different hierarchical topographies under various spinning rates to determine the role of structure in lubricant retention, tracking changes in contact hysteresis and sliding angles for both water and ethanol in relation to lubricant loss [201]. The most effective structure at retaining lubricant was shown to be one with uniform nano-features (Fig. 20).

Schellenberger et al. recently published images of the shape of drops on lubricant-infused surfaces by laser scanning confocal microscopy [198]. Fig. 21 shows the cross sectional image of a water drop on a salinized glass micro-pillar array, with and without an infused ionic liquid, one of three chosen lubricating liquids. This comparison highlights the impact of the impregnated liquid in replacing the air in the micro-structure. The correct contact angle of the drop–pillar interface in the lubricant could be imagined only through confocal microscopy, and was found to be 140° while the macroscopic contact angle appeared to be 60° due to the lubricant cloaking the sessile droplet. On these surfaces, water drops slid off easily on top of the infused solvent interfacing with the drop.

5.4. Improvements on existing methods

Recent publications in the field of superhydrophobicity have made substantial improvements towards producing robust versions of the existing techniques covered in this review. Some highlighted works include, fabrics for oil and water separation [202], hierarchical patterned steel surfaces [203], magnesium alloys [204], and titanium dioxide nano-particles [205]. These publications report extensive robustness testing specific to their material's targeted end use, and are examples the field's progress towards producing superhydrophobicity with clear practical applications in mind.

6. Robustness testing methods

The generic term ‘robustness’ is used often in the literature, and can refer to different aspects of surface robustness. The main areas of interest are thermodynamic, mechanical, and chemical robustness, and these are tested in different ways depending on the intended application/area of expertise. In each case, a common means to determine the damage to the superhydrophobic state between tests is to monitor changes in the static contact angle and contact angle hysteresis.

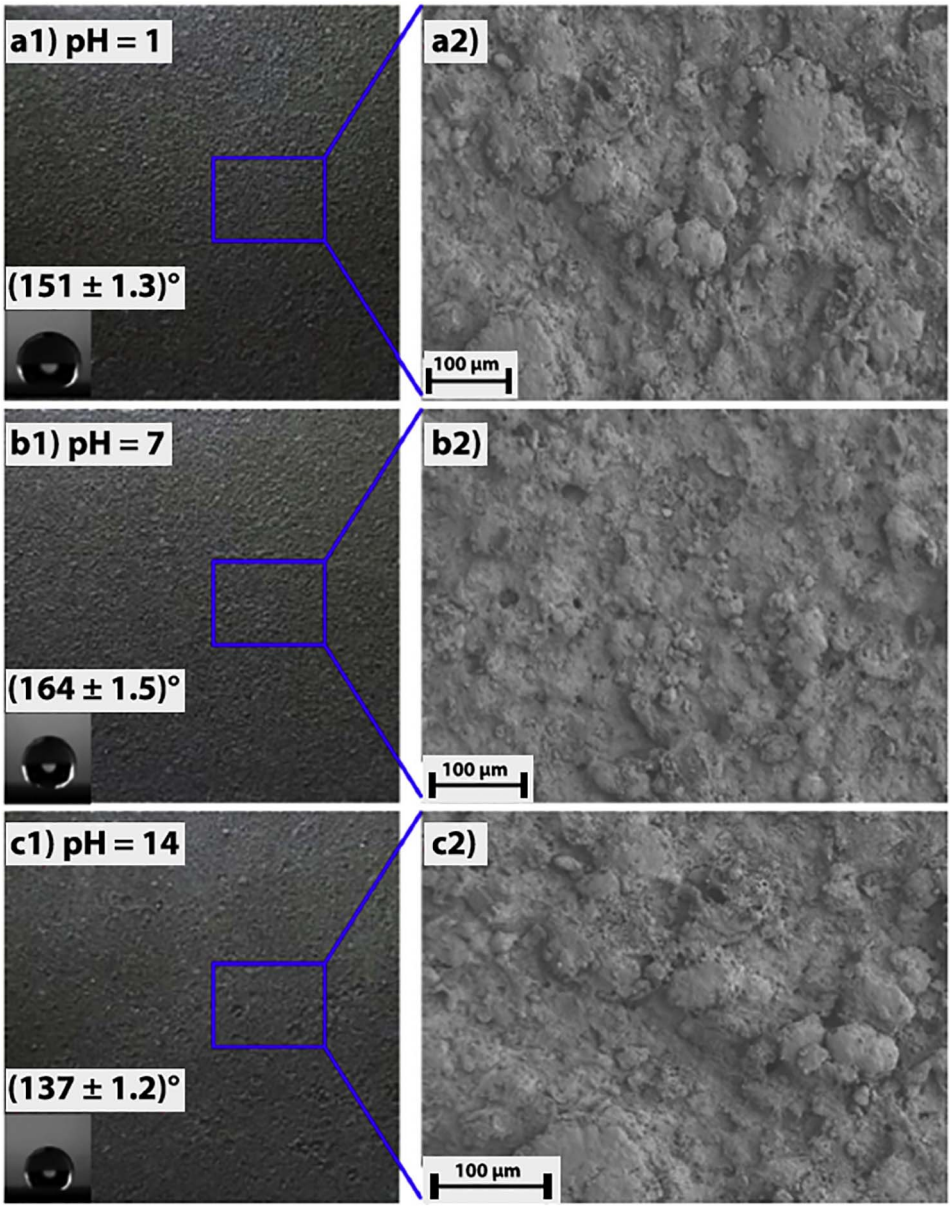

Fig. 22. Superhydrophobic coatings immersed in acidic (pH = 1), neutral (pH = 7) and alkaline (pH = 14) solutions for 15 days. Reprinted from [216], Copyright 2015, with permission from Elsevier.

6.1. Thermodynamic robustness

Some studies have focused on applying pressure on the plastron and investigating its stability, including using compression tests [58,169,206], immersion tests or stability tests [13,207,208], (with and without shear force), and droplet bouncing/impact tests [58,169,209–212]. Plastron reflectivity can be monitored with confocal microscopy, force applied can be tracked during compression cycles, and number of droplet bounces can be counted in droplet impact. Several relevant methods testing thermodynamic robustness of the Cassie state were reviewed in the Section on Thermodynamic and kinetic robustness.

6.2. Chemical robustness

Chemical robustness focuses on two aspects of a superhydrophobic surface, topography and surface energy damage. In particular, surface energy damage involves the removal of self-assembled layers or modification of existing surface chemistry resulting in a decrease in hydrophobicity. Chemical robustness is typically tested by corrosion exposure (acidic and basic) [168,200,202,203,213–218], and UV exposure [200,203,214,215,219,220]. More specific tests have also been performed for resistance to different solvents [221,222]. During these tests, the change in surface wettability is often monitored and compared to the topography damage by SEM micrographs, and potential change in surface chemistry by X-ray photoelectric spectroscopy (XPS).

Wang et al. performed comprehensive corrosion resistance tests on their superhydrophobic surfaces, comprised of a polyvinylidene fluoride (PVDF)/fluorinated ethylene propylene (FEP)/carbon nanofibers (CNFs) composite coating [216]. Tests were performed by immersing the prepared coatings at different pH conditions over a period of 15 days (Fig. 22). The water contact angle on these surfaces decreased from 164° to 151° under strongly acidic conditions, and to 137° in strongly alkaline conditions.

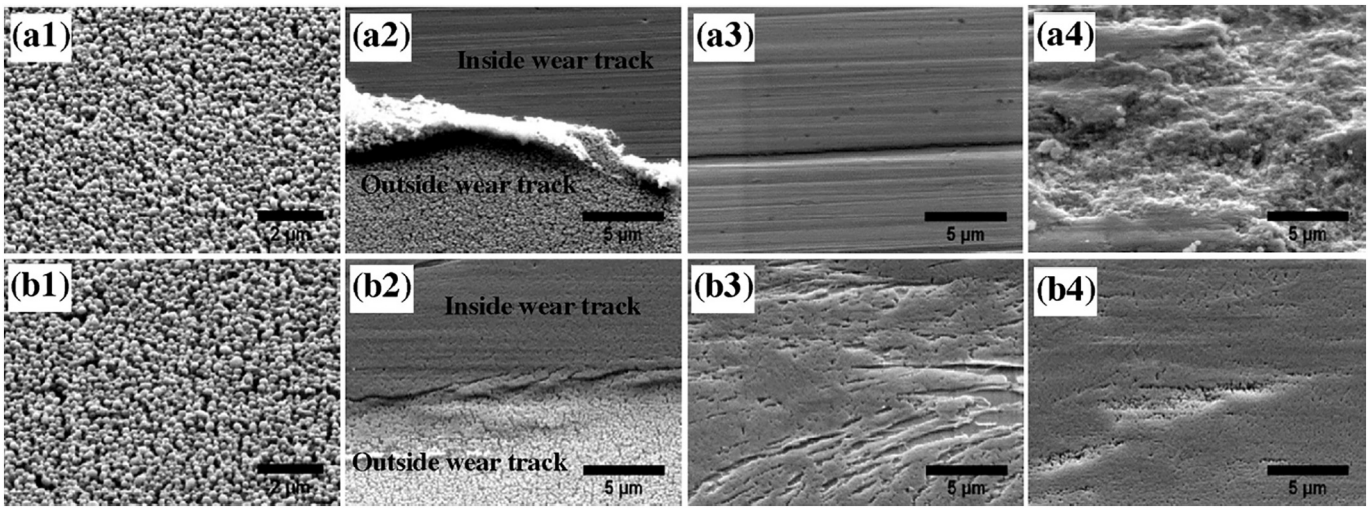

Fig. 23. PTFE coated sample (a1) intact surface, (a2) After 10 rubbing cycles, edge of the wear track, (a3) 10 rubbing cycles, center of the wear track, and (a4) 1000 rubbing cycles, center of the wear track; PDA/PTFE coated sample (b1) intact surface, (b2) 10 rubbing cycles, edge of the wear track, (b3) 10 rubbing cycles, center of the wear track, and (b4) 1000 rubbing cycles, center of the wear track. Reprinted from [229], Copyright 2013, with permission from Elsevier.

6.3. Mechanical robustness

Mechanical robustness refers to changes to the micro- and nano-scale topography when exposed to physical damage, and its standardization is an area of current discussion. Common techniques to induce damage include abrasion tests, cavitation tests, nano-indentation, scratching, tensile strength tests and adhesion tests.

Abrasion and jet tests are performed to emulate exposure to friction forces, particularly when exposed to environmental conditions including sand abrasion from wind. Sand abrasion can be simulated by dropping silica particles from heights or by vibrating the particles on the surface; sandpaper abrasion, or using a tribometer to control the amount of wear force applied with depth of penetration [16,18,19,203,213–216,219,223–225]. More recently, abrasion tests have also been performed using water jet tests which test the thermodynamic robustness of the trapped air in the surface roughness and its mechanical resistance to shearing forces [226,227], and tests emulating fog and rain droplets [228].

Beckford and Zou et al. performed abrasion tests on poly tetrafluoroethylene (PTFE) thin films coated on stainless steel with and without a polydopamine (PDA) adhesive layer [229]. Friction and wear resistance was determined using a tribometer with a ball on flat configuration, measuring up to 1000 rubbing cycles (Fig. 23). The addition of the adhesive layer increased the abrasion resistance of the composite layer by 500 times, which was confirmed using X-ray photoelectron spectroscopy (XPS).

Cavitation tests are performed with the surface immersed in water under sonication for prolonged times resulting in damage across the topography due to the formation and explosion of air bubbles, which release extremely high heat and high shear locally. Surface wettability is often monitored at time intervals of cavitation to track damage to the superhydrophobicity [19,230,231].

Emelyanenko et al. prepared a superhydrophobic coating on stainless steel for use in heavily loaded hydraulic systems [19]. The required surface roughness was produced via nanosecond IR laser treatment, followed by chemisorption of fluorooxysilane. Cavitation tests were performed over 90 min periods with an ultrasonic water bath, which resulted in removal of micro- and nano-sized particles (Fig. 24). Static contact angles and roll off angles were monitored over the course of cavitation, revealing an overall increase in water adhesion due to increased Wenzel wetting.

Nano-indentation and scratch tests are used to determine the hardness and resistance to an applied force. Force measurements can also provide quantitative data on mechanical properties [232–236]. A cruder scratch test can be done via applying a pencil to the surface, and such an industry standard for coatings exists [168,206,213]. This is a significantly more qualitative approach, but allows for a comparison to standard industry coatings. These tests, designed for flat surfaces, are not well suited to obtain quantitative mechanical properties of rough topographies which are characteristic for superhydrophobic surfaces, because of their sensitivity to depth of film penetration [237,238]. Due to this challenge, the example chosen is a standard flat surface. Attempts to utilize these techniques for complex rough superhydrophobic surfaces were performed by Scarratt et al. [188], who highlighted the challenges that need to be overcome when using these highly sensitive techniques. Errors in nano-indentation measurements on rough substrates are notoriously large [236], and nano-scratch tests on rough surfaces are not commonly performed.

Fang et al. determined the nano-mechanical characteristics of Si and GaAs using nano-indentation and nano-scratch techniques (Fig. 25) [234]. The mechanical properties were calculated from the loading–unloading curve at various loading force. The hardness of the material was evaluated by obtaining the wear properties and volume removal rate. Fig. 25 shows nano-scratches at different applied loads on both Si and GaAs.

Other tests for mechanical robustness include: adhesion tests, which are often performed by the application of a known grade of sticky tape to the substrate [203,206,213,215,216,219], tensile strength tests [209,211,215,239], and vibrational testing [240,241], which monitors the change in wettability as the surface is exposed to vibrations.

A recent review highlights the variety of different mechanical wear tests performed on superhydrophobic surfaces in the last 5 years, in an aim to create more systematic robustness testing methods for accurate assessment for industrial application [54]. They address variations in superhydrophobic fabrication methods and how this affects their subsequent robustness. An ideal surface is one that retains its geometric features required for trapping air in its micro- and nano- structure, while maintaining its hydrophobic surface chemistry. In this respect, using hydrophobic materials and inducing roughened features is most effective in fulfilling these criteria. However, the choice of materials and geometries taken, in addition to adhesion to the substrate greatly affects the overall mechanical robustness.

In regards to ideal superhydrophobic surface design, the degree of water penetration into the micro-/nano-scale structure via Laplace pressure is heavily influenced by spacing and height of features [242–247]. The presence of double scale roughness can assist in

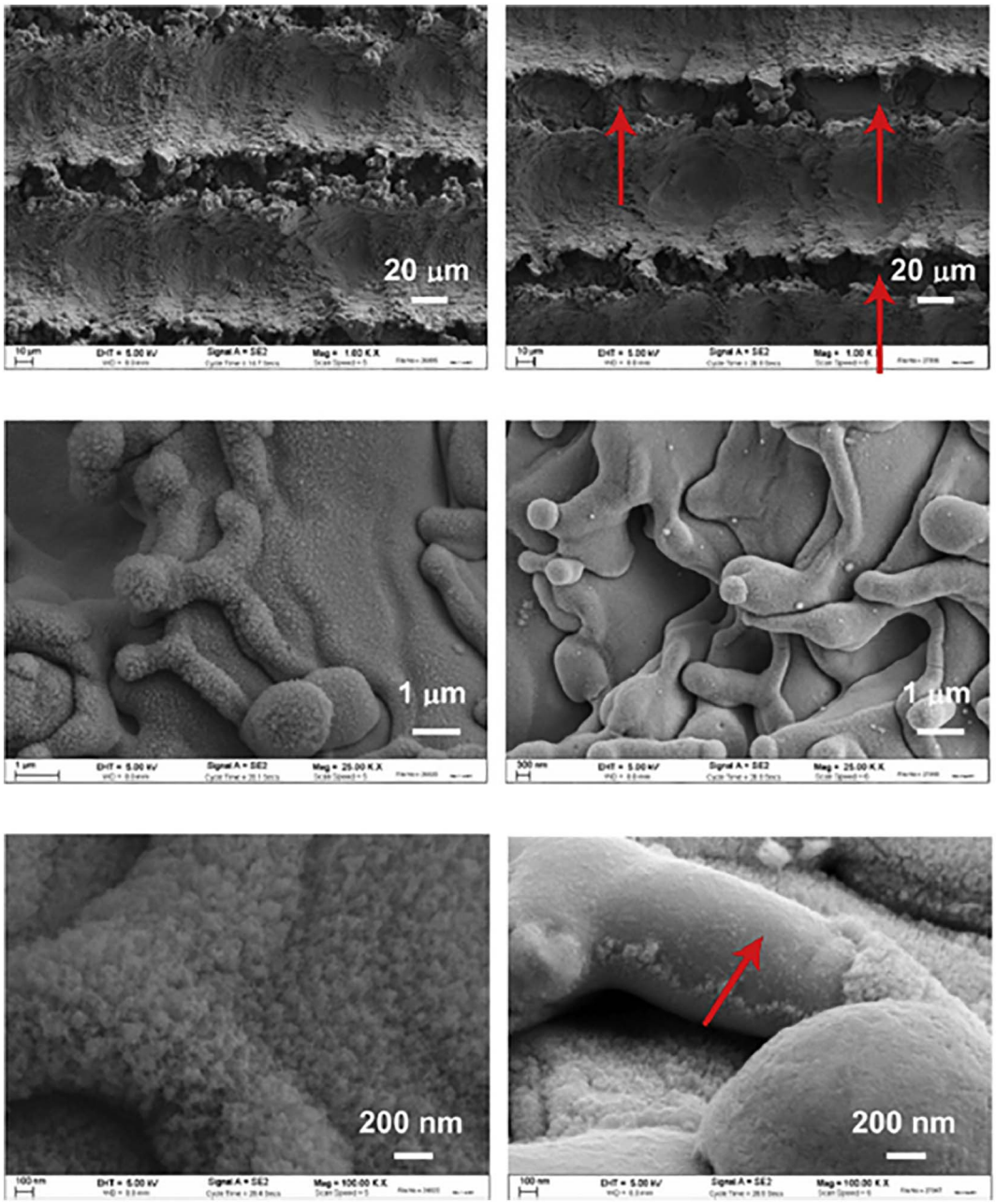

Fig. 24. A superhydrophobic coating on stainless steel before cavitation (left panels), and after a 90-min of exposure to cavitation test (right panels). The red arrows indicate the areas where the micro- and nano-sized particles were removed by cavitation. Reprinted from [19], Copyright 2015, with permission from Elsevier. (For interpretation of the references to color in this figure legend, the reader is referred to the web version of this article.)

creating an improved geometry for trapping air between the drop and the surface, thus enhancing stability [248–250]. A robust superhydrophobic surface needs to be able to resist chemical, and mechanical damage, while demonstrating overall thermodynamic stability. If the geometry or surface chemistry is compromised, then the surface properties will degrade and superhydrophobicity will be lost. Self-healing surfaces and SLIPS are alternative approaches reducing thermodynamic and mechanical robustness limitations. An alternative is the optimization of simple fabrication methods to produce the most effective topography for a stable Cassie state on an already hydrophobic material. There is still much work to be done in the field before large scale application of robust and durable superhydrophobic surfaces can be a reality.

7. Conclusions

This review focused on the long term stability of fabricated superhydrophobic surfaces, focusing especially on the work published in the past 15 years. Particular attention was devoted to the stability of the Cassie wetting state, the physical mechanism used to induce the required surface chemistry and nano- and micro-structure, and how the fabrication directly affected the durability of the surfaces. Although the field of superhydrophobic surfaces has seen great progress over the past twenty years, many problems still need to be resolved in order to achieve realistic technological applications. A true superhydrophobic state, which brings most of the desired advantages, requires a relatively stable Cassie state, with air trapped in the roughness of the surface. As a minimum requirement, all surfaces purporting 'superhydrophobic' properties should report values of contact angle hysteresis, and relate

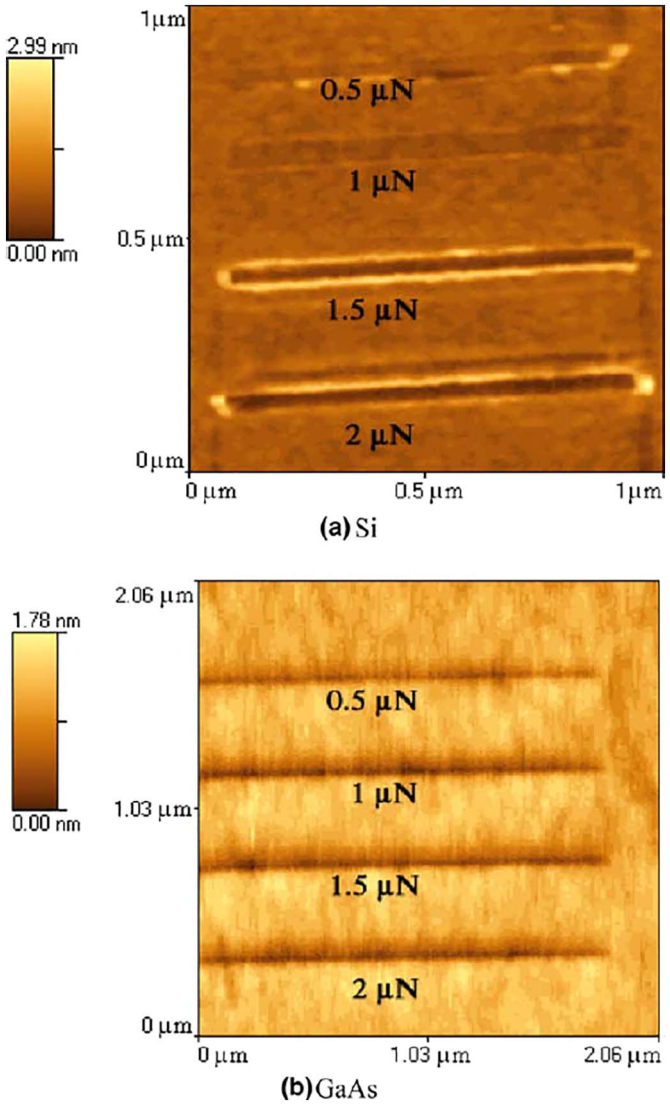

Fig. 25. Scratches in (a) Si and (b) GaAs surfaces upon various applied loadings. Reprinted from [234], Copyright 2005, with permission from Elsevier.

these to the likely wetting state of the surface before and after use, or upon application of wear. In order for the field to progress, a thorough characterization of mechanical and thermodynamic stability of the superhydrophobic state in the desired conditions of use must be performed. More easily accessible and standardized methods must be developed for testing the robustness of very rough surfaces under pressure, wear, scratch, immersion, exposure to contamination, and other conditions. Existing methods are mostly applicable to smooth surfaces, so the errors involved in applying the methods to very rough surfaces are large. In order to achieve realistic applications, the cost of fabrication on a large scale should be addressed, and lower cost, single-step alternatives explored. In the future, a closer and more direct collaboration between researchers from different disciplines, including from industry, will benefit the development of more robust and truly applicable super-repellent structured surfaces.

Acknowledgments

This research was supported by an Australian Government Research Training Program (RTP), and Surface Coatings Association Australia Scholarship.

References

[1] Quéré D. Wetting and roughness. Annu Rev Mater Res 2008;38:71–99. [Palo Alto: Annual Reviews].
[2] Neinhuis C, Barthlott W. Ann Bot 1997;79:667–77.
[3] Blossey R. Nat Mater 2003;2:301–6.
[4] Quéré D. Rep Prog Phys 2005;68:2495–532.
[5] Tuteja A, Choi W, Ma M, Mabry JM, Mazzella SA, Rutledge GC, et al. Science 2007;318:1618–22.
[6] Marmur A. Langmuir 2004;20:3517–9.
[7] Gao L, McCarthy TJ. Langmuir 2006;22:2966–7.
[8] Cassie ABD, Baxter S. Trans Faraday Soc 1944;40:0546–50.
[9] Lee T, Charrault E, Neto C. Adv Colloid Interf Sci 2014;210:21–38.
[10] Lafuma A, Quéré D. Nat Mater 2003;2:457–60.
[11] Callies M, Quéré D. Soft Matter 2005;1:55–61.
[12] Zhang P, Lv FY. Energy 2015;82:1068–87.
[13] Poetes R, Holtzmann K, Franze K, Steiner U. Phys Rev Lett 2010;105:166104.
[14] Deng X, Mammen L, Butt HJ, Vollmer D. Science 2012;335:67–70.
[15] Zhou H, Wang H, Niu H, Gestos A, Lin T. Adv Funct Mater 2013;23:1664–70.
[16] Li Y, Chen SS, Wu MC, Sun JQ. Adv Mater 2014;26. [3344-+].
[17] Shillingford C, MacCallum N, Wong TS, Kim P, Aizenberg J. Nanotechnology 2014;25:12.
[18] Huovinen E, Takkunen L, Korpela T, Suvanto M, Pakkanen TT, Pakkanen TA. Langmuir 2014;30:1435–43.
[19] Emelyanenko AM, Shagieva FM, Domantovsky AG, Boinovich LB. Appl Surf Sci 2015;332:513–7.
[20] Kavalenka MN, Vüllers F, Lischker S, Zeiger C, Hopf A, Röhrig M, et al. ACS Appl Mater Interfaces 2015;7:10651–5.
[21] Bocquet L, Lauga E. Nat Mater 2011;10:334–7.
[22] Johnson R, Dettre R. Contact angle, wettability, and adhesion. Adv Chem Ser 1964;vol. 43:112.
[23] Young T. Phil Trans R Soc London 1805;95:65–87.
[24] Dettre RH, Johnson Jr. RE. Adv Chem Ser 1963;43:136–44.
[25] Marmur A. Langmuir 2003;19:8343–8.
[26] Bartolo D, Bouamrirene F, Verneuil E, Buguin A, Silberzan P, Moulinet S. Europhys Lett 2006;74:299–305.
[27] Kwon H-M, Paxson AT, Varanasi KK, Patankar NA. Phys Rev Lett 2011;106:036102.
[28] Bormashenko E, Pogreb R, Whyman G, Erlich M. Langmuir 2007;23:6501–3.
[29] Reyssat M, Yeomans JM, Quéré D. Europhys Lett 2008;81:26006.
[30] Tsai P, Lammertink RGH, Wessling M, Lohse D. Phys Rev Lett 2010;104:116102.
[31] Poetes RM. Dynamic and static conformations at the water-solid interface [PhD Thesis]. UK: University of Cambridge; 2009.
[32] Krupenkin TN, Taylor JA, Wang EN, Kolodner P, Hodes M, Salamon TR. Langmuir 2007;23:9128–33.
[33] Boreyko JB, Chen C-H. Phys Rev Lett 2009;103:174502.
[34] Herminghaus S. Europhys Lett 2000;52:165.
[35] Bobji MS, Kumar SV, Asthana A, Govardhan RN. Langmuir 2009;25:12120–6.
[36] Epstein PS, Plesset MS. J Chem Phys 1950;18:1505–9.
[37] Samaha MA, Ochanda FO, Tafreshi HV, Tepper GC, Gad-el-Hak M. Rev Sci Instrum 2011;82:045109.
[38] Lv P, Xue Y, Shi Y, Lin H, Duan H. Phys Rev Lett 2014;112:196101.
[39] Lee C, Kim C-J. Phys Rev Lett 2011;106:014502.
[40] Krupenkin T, Taylor JA, Wang E, Kolodner P, Hodes Marc, Salamon T. Langmuir 2007;23:9128–33.
[41] Adera S, Raj R, Enright R, Wang EN. Nat Commun 2013;4:2518.
[42] Forsberg P, Nikolajeff F, Karlsson M. Soft Matter 2011;7:104–9.
[43] Verho T, Korhonen JT, Sainiemi L, Jokinen V, Bower C, Franze K, et al. Proc Natl Acad Sci U S A 2012;109:10210–3.
[44] Lei L, Li H, Shi J, Chen Y. Langmuir 2010;26:3666–9.
[45] Lee J, Yong K. NPG Asia Mater 2015;7:e201.
[46] Checco A, Ocko BM, Rahman A, Black CT, Tasinkevych M, Giacomello A, et al. Phys Rev Lett 2014;112:216101.
[47] Sun W, Zhou SX, You B, Wu LM. J Mater Chem A 2013;1:3146–54.
[48] Liu JL, Feng XQ, Wang GF, Yu SW. J Phys Condens Matter 2007;19:12.
[49] Cao LL, Hu HH, Gao D. Langmuir 2007;23:4310–4.
[50] Zhang B, Zhang XR. Langmuir 2015;31:9448–57.
[51] Ems H, Ndao S. Appl Surf Sci 2015;339:137–43.
[52] Cassie ABD, Baxter S. Trans Faraday Soc 1944;40:546–51.
[53] Li XM, Reinhoudt D, Crego-Calama M. Chem Soc Rev 2007;36:1350–68.
[54] Milionis A, Loth E, Bayer IS. Adv Colloid Interf Sci 2016;229:57–79.
[55] Furstner R, Barthlott W, Neinhuis C, Walzel P. Langmuir 2005;21:956–61.
[56] Wong T-S, Huang AP-H, Ho C-M. Langmuir 2009;25:6599–603.
[57] Wang JZ, Zheng ZH, Li HW, Huck WTS, Sirringhaus H. Nat Mater 2004;3:171–6.
[58] Kwon Y, Patankar N, Choi J, Lee J. Langmuir 2009;25:6129–36.
[59] Long CJ, Schumacher JF, Brennan AB. Langmuir 2009;25:12982–9.
[60] Steinberger A, Cottin-Bizonne C, Kleimann P, Charlaix E. Nat Mater 2007;6:665–8.
[61] Kim T-I, Baek Ch, Suh KY, Seo S-M, Lee HH. Small 2008;4:182–5.
[62] Jung YC, Bhushan B. Langmuir 2009;25:9208–18.
[63] Reyssat M, Quéré D. J Phys Chem B 2009;113:3906–9.
[64] He B, Lee J, Patankar NA. Colloids Surf A Physicochem Eng Asp 2004;248:101–4.
[65] Jung YC, Bhushan B. ACS Nano 2009;3:4155–63.
[66] Zhang X, Zhang J, Ren Z, Li X, Zhang X, Zhu D, et al. Langmuir 2009;25:7375–82.
[67] Lee S-M, Kwon TH. J Micromech Microeng 2007;17:687–92.
[68] Choi Y-W, Han J-E, Lee S, Sohn D. Macromol Res 2009;17:821–4.

[69] Barthlott W, Neinhuis C, Cutler D, Ditsch F, Meusel I, Theisen I, et al. Bot J Linn Soc 1998;126:237–60.
[70] Lee SM, Kwon TH. Nanotechnology 2006;17:3189–96.
[71] Suh KY, Kim YS, Lee HH. Adv Mater 2001;13:1386–9.
[72] Jeong HE, Lee SH, Kim JK, Suh KY. Langmuir 2006;22:1640–5.
[73] Sun MH, Luo CX, Xu LP, Ji H, Qi OY, Yu DP, et al. Langmuir 2005;21:8978–81.
[74] Cho WK, Choi IS. Adv Funct Mater 2008;18:1089–96.
[75] Lee W, Jin MK, Yoo WC, Lee JK. Langmuir 2004;20:7665–9.
[76] Neto C, Joseph KR, Brant WR. Phys Chem Chem Phys 2009;11:9537–44.
[77] Autumn K, Liang YA, Hsieh ST, Zesch W, Chan WP, Kenny TW, et al. Nature 2000;405:681–5.
[78] Jin MH, Feng XJ, Feng L, Sun TL, Zhai J, Li TJ, et al. Adv Mater 2005;17. [1977-+].
[79] Berendsen CWJ, Skeren M, Najdek D, Cerny F. Appl Surf Sci 2009;255:9305–10.
[80] Winkleman A, Gotesman G, Yoffe A, Naaman R. Nano Lett 2008;8:1241–5.
[81] Manca M, Cortese B, Viola I, Arico AS, Cingolani R, Gigli G. Langmuir 2008;24:1833–43.
[82] Teshima K, Sugimura H, Inoue Y, Takai O, Takano A. Appl Surf Sci 2005;244:619–22.
[83] Teshima K, Sugimura H, Inoue Y, Takai O, Takano A. Chem Vap Depos 2004;10. [295-+].
[84] Wu YY, Bekke M, Inoue Y, Sugimura H, Kitaguchi H, Liu CS, et al. Thin Solid Films 2004;457:122–7.
[85] Cicala G, Milella A, Palumbo E, Favia P, d'Agostino R. Diam Relat Mater 2003;12:2020–5.
[86] Wu YY, Kuroda M, Sugimura H, Inoue Y, Takai O. Surf Coat Technol 2003;174:867–71.
[87] Wu YY, Sugimura H, Inoue Y, Takai O. Thin Solid Films 2003;435:161–4.
[88] Fresnais J, Benyahia L, Poncin-Epaillard F. Surf Interface Anal 2006;38:144–9.
[89] Kim JW, Kim CJ, Ieee I. Nanostructured surfaces for dramatic reduction of flow resistance in droplet-based microfluidics. Fifteenth IEEE intern. conf. micro electro mechanical systems, technical digest. 2002; 2002. p. 479–82.
[90] Shiu JY, Kuo CW, Chen PL, Mou CY. Chem Mater 2004;16:561–4.
[91] Lim H, Jung D-H, Noh J-H, Choi G-R, Kim W-D. Chin Sci Bull 2009;54:3613–6.
[92] Minko S, Muller M, Motornov M, Nitschke M, Grundke K, Stamm M. J Am Chem Soc 2003;125:3896–900.
[93] Balu B, Breedveld V, Hess DW. Langmuir 2008;24:4785–90.
[94] Shen P, Uesawa N, Inasawa S, Yamaguchi Y. Langmuir 2010;26:13522–7.
[95] Qian BT, Shen ZQ. Langmuir 2005;21:9007–9.
[96] Lee J-P, Choi S, Park S. Langmuir 2011;27:809–14.
[97] Kim BS, Shin S, Shin SJ, Kim KM, Cho HH. Langmuir 2011;27:10148–56.
[98] Liu H, Feng L, Zhai J, Jiang L, Zhu DB. Langmuir 2004;20:5659–61.
[99] Li M, Zhai J, Liu H, Song YL, Jiang L, Zhu DB. J Phys Chem B 2003;107:9954–7.
[100] Zhang X, Shi F, Yu X, Liu H, Fu Y, Wang ZQ, et al. J Am Chem Soc 2004;126:3064–5.
[101] Wang J, Li A, Chen H, Chen D. J Bionic Eng 2011;8:122–8.
[102] He G, Wang K. Appl Surf Sci 2011;257:6590–4.
[103] Hosono E, Fujihara S, Honma I, Zhou HS. J Am Chem Soc 2005;127:13458–9.
[104] Wu XD, Zheng LJ, Wu D. Langmuir 2005;21:2665–7.
[105] Zhao N, Shi F, Wang ZQ, Zhang X. Langmuir 2005;21:4713–6.
[106] Larmour IA, Saunders GC, SEJ Bell. New J Chem 2008;32:1215–20.
[107] Feng X, Feng L, Jin M, Zhai J, Jiang L, Zhu D. J Am Chem Soc 2004;126:62–3.
[108] Zhao Y, Li M, Lu Q, Shi Z. Langmuir 2008;24:12651–7.
[109] Hsieh C-T, Chen W-Y, Wu F-L, Shen Y-S. J Adhes Sci Technol 2008;22:265–75.
[110] Sun C, Ge L-Q, Gu Z-Z. Thin Solid Films 2007;515:4686–90.
[111] Lai Y, Huang Y, Wang H, Huang J, Chen Z, Lin C. Colloids Surf B 2010;76:117–22.
[112] Sato O, Kubo S, Gu Z-Z. Acc Chem Res 2009;42:1–10.
[113] Bravo J, Zhai L, Wu Z, Cohen RE, Rubner MF. Langmuir 2007;23:7293–8.
[114] Lvov Y, Ariga K, Onda M, Ichinose I, Kunitake T. Langmuir 1997;13:6195–203.
[115] Ling XY, Phang IY, Vancso GJ, Huskens J, Reinhoudt DN. Langmuir 2009;25:3260–3.
[116] Manca M, Cannavale A, De Marco L, Arico AS, Cingolani R, Gigli G. Langmuir 2009;25:6357–62.
[117] Liu YY, Chen XQ, Xin JH. Nanotechnology 2006;17:3259–63.
[118] Lai Y, Lin Z, Huang J, Sun L, Chen Z, Lin C. New J Chem 2010;34:44–51.
[119] Amigoni S, de Givenchy ET, Dufay M, Guittard F. Langmuir 2009;25:11073–7.
[120] Motornov M, Sheparovych R, Lupitskyy R, MacWilliams E, Minko S. Adv Mater 2008;20. [200-+].
[121] Zhang G, Wang DY, Gu ZZ, Mohwald H. Langmuir 2005;21:9143–8.
[122] Shen Y, Wang J, Kuhlmann U, Hildebrandt P, Ariga K, Moehwald H, et al. Chem Eur J 2009;15:2763–7.
[123] Telford AM, Hawkett BS, Such C, Neto C. Chem Mater 2013;25:3472–9.
[124] Velikov KP, Christova CG, Dullens RPA, van Blaaderen A. Science 2002;296:106–9.
[125] Vericat C, Benitez GA, Grumelli DE, Vela ME, Salvarezza RC. J Phys Condens Matter 2008;20.
[126] Vericat C, Vela ME, Benitez G, Carro P, Salvarezza RC. Chem Soc Rev 2010;39:1805–34.
[127] Soeno T, Inokuchi K, Shiratori S. Appl Surf Sci 2004;237:543–7.
[128] Jindasuwan S, Nimittrakoolchai O, Sujaridworakun P, Jinawath S, Supothina S. Thin Solid Films 2009;517:5001–5.
[129] Zhai L, Cebeci FC, Cohen RE, Rubner MF. Nano Lett 2004;4:1349–53.
[130] Han JT, Xu XR, Cho KW. Langmuir 2005;21:6662–5.
[131] Zhang LB, Chen H, Sun JQ, Shen JC. Chem Mater 2007;19:948–53.
[132] Ma ML, Hill RM, Lowery JL, Fridrikh SV, Rutledge GC. Langmuir 2005;21:5549–54.
[133] Zhu M, Zuo W, Yu H, Yang W, Chen Y. J Mater Sci 2006;41:3793–7.
[134] Wang N, Zhao Y, Jiang L. Macromol Rapid Commun 2008;29:485–9.
[135] Huang ZM, Zhang YZ, Kotaki M, Ramakrishna S. Compos Sci Technol 2003;63:2223–53.
[136] Acatay K, Simsek E, Ow-Yang C, Menceloglu YZ. Angew Chem Int Ed 2004;43:5210–3.
[137] Ma ML, Mao Y, Gupta M, Gleason KK, Rutledge GC. Macromolecules 2005;38:9742–8.
[138] Zheng J, He A, Li J, Xu J, Han CC. Polymer 2006;47:7095–102.
[139] Mizukoshi T, Matsumoto H, Minagawa M, Tanioka A. J Appl Polym Sci 2007;103:3811–7.
[140] Gu G, Tian Y, Li Z, Lu D. Appl Surf Sci 2011;257:4586–8.
[141] Li Z, Zheng Y, Cui L. J Coat Technol Res 2012;9:579–87.
[142] Wu W, Wang X, Liu X, Zhou F. ACS Appl Mater Interfaces 2009;1:1656–61.
[143] Burkarter E, Saul CK, Thomazi F, Cruz NC, Zanata SM, Roman LS, et al. J Phys D Appl Phys 2007;40:7778–81.
[144] Sahoo BN, Sabarish B, Balasubramanian K. Prog Org Coat 2014;77:904–7.
[145] Burkarter E, Saul CK, Thomazi F, Cruz NC, Roman LS, Schreiner WH. Surf Coat Technol 2007;202:194–8.
[146] van der Wal P, Steiner U. Soft Matter 2007;3:426–9.
[147] Zhang Y-Y, Ge Q, Yang L-L, Shi X-J, Li J-J, Yang D-Q, et al. Appl Surf Sci 2015;339:151–7.
[148] van der Wal BP. Static and dynamic wetting of porous Teflon® surfaces [PhD Thesis]. University of Groningen; 2006.
[149] Nilsson MA, Daniello RJ, Rothstein JP. J Phys D Appl Phys 2010;43:5.
[150] Hikita M, Tanaka K, Nakamura T, Kajiyama T, Takahara A. Langmuir 2005;21:7299–302.
[151] Shang HM, Wang Y, Limmer SJ, Chou TP, Takahashi K, Cao GZ. Thin Solid Films 2005;472:37–43.
[152] Xiu Y, Xiao F, Hess DW, Wong CP. Thin Solid Films 2009;517:1610–5.
[153] Tadanaga K, Kitamuro K, Matsuda A, Minami T. J Sol-Gel Sci Technol 2003;26:705–8.
[154] Rao AV, Latthe SS, Nadargi DY, Hirashima H, Ganesan V. J Colloid Interface Sci 2009;332:484–90.
[155] Tadanaga K, Morinaga J, Minami T. J Sol-Gel Sci Technol 2000;19:211–4.
[156] Doshi DA, Shah PB, Singh S, Branson ED, Malanoski AP, Watkins EB, et al. Langmuir 2005;21:7805–11.
[157] Chen H, Yuan Z, Zhang J, Liu Y, Li K, Zhao D, et al. J Porous Mater 2009;16:447–51.
[158] Li XH, Chen GM, Ma YM, Feng L, Zhao HZ, Jiang L, et al. Polymer 2006;47:506–9.
[159] Shirtcliffe NJ, McHale G, Newton MI, Perry CC. Langmuir 2003;19:5626–31.
[160] Nakajima A, Abe K, Hashimoto K, Watanabe T. Thin Solid Films 2000;376:140–3.
[161] Song W, Veiga DD, Custodio CA, Mano JF. Adv Mater 2009;21. [1830-+].
[162] Xie QD, Xu J, Feng L, Jiang L, Tang WH, Luo XD, et al. Adv Mater 2004;16. [302-+].
[163] Zhao N, Xie QD, Weng LH, Wang SQ, Zhang XY, Xu J. Macromolecules 2005;38:8996–9.
[164] Xie QD, Fan GQ, Zhao N, Guo XL, Xu J, Dong JY, et al. Adv Mater 2004;16. [1830-+].
[165] Chen HJ, Zhu YF, Zhang Y, Xu JR. Spectrosc Spectr Anal 2008;28:1799–802.
[166] Qian H, Zhu YF, Xu JR. Spectrosc Spectr Anal 2003;23:708–13.
[167] Lianbin Z, Yang L, Junqi S, Jiacong S. J Colloid Interface Sci 2008;319:302–8.
[168] Xu LG, Geng Z, He JH, Zhou G. ACS Appl Mater Interfaces 2014;6:9029–35.
[169] Xu LY, Zhu DD, Lu XM, Lu QH. J Mater Chem A 2015;3:3801–7.
[170] Xu L, Karunakaran RG, Guo J, Yang S. ACS Appl Mater Interfaces 2012;4:1118–25.
[171] Liu M, Jiang L. Adv Funct Mater 2010;20:3753–64.
[172] Rosario R, Gust D, Garcia AA, Hayes M, Taraci JL, Clement T, et al. J Phys Chem B 2004;108:12640–2.
[173] Zhou X, Zhang Z, Men X, Yang J, Xu X, Zhu X, et al. Appl Surf Sci 2011;258:285–9.
[174] Pan J, Song X, Zhang J, Shen H, Xiong Q. J Phys Chem C 2011;115:22225–31.
[175] Jiang WH, Wang GJ, He YN, Wang XG, An YL, Song YL, et al. Chem Commun 2005:3550–2.
[176] Yang J, Zhang Z, Men X, Xu X, Zhu X. Colloids Surf A Physicochem Eng Asp 2010;367:60–4.
[177] Li Y, Li L, Sun J. Angew Chem Int Ed 2010;49:6129–33.
[178] Wang H, Xue Y, Ding J, Feng L, Wang X, Lin T. Angew Chem Int Ed 2011;50:11433–6.
[179] Wang X, Liu X, Zhou F, Liu W. Chem Commun 2011;47:2324–6.
[180] Xue C-H, Ma J-Z. J Mater Chem A 2013;1:4146–61.
[181] Youngblood JPS, N. R.. MRS Bull 2008;33:732–41.
[182] Kim JB, Kim P, Pegard NC, Oh SJ, Kagan CR, Fleischer JW, et al. Nat Photonics 2012;6:327–32.
[183] Genzer J, Groenewold J. Soft Matter 2006;2:310–23.
[184] Greco F, Fujie T, Ricotti L, Taccola S, Mazzolai B, Mattoli V. ACS Appl Mater Interfaces 2013;5:573–84.
[185] Breid D, Crosby AJ. Soft Matter 2011;7:4490–6.
[186] Fu C-C, Grimes A, Long M, Ferri CGL, Rich BD, Ghosh S, et al. Adv Mater 2009;21. [4472-+].
[187] Manna U, Carter MCD, Lynn DM. Adv Mater 2013;25:3085–9.
[188] Scarratt LRJ, Hoatson BS, Wood ES, Hawkett BS, Neto C. ACS Appl Mater Interfaces 2016;8:6743–50.
[189] Xue C-H, Zhang Z-D, Zhang J. Jia S-T. J Mater Chem A 2014;2:15001–7.
[190] Bohn HF, Federle W. Proc Natl Acad Sci U S A 2004;101:14138–43.
[191] Lalia BS, Anand S, Varanasi KK, Hashaikeh R. Langmuir 2013;29:13081–8.
[192] Kim P, Wong T-S, Alvarenga J, Kreder MJ, Adorno-Martinez WE, Aizenberg J. ACS Nano 2012;6:6569–77.

[193] Zhang P, Chen H, Zhang L, Ran T, Zhang D. Appl Surf Sci 2015;355:1083–90.
[194] Xiao L, Li J, Mieszkin S, Di Fino A, Clare AS, Callow ME, et al. ACS Appl Mater Interfaces 2013;5:10074–80.
[195] Yang S, Qiu R, Song H, Wang P, Shi Z, Wang Y. Appl Surf Sci 2015;328:491–500.
[196] Wang P, Lu Z, Zhang D. Corros Sci 2015;93:159–66.
[197] Smith JD, Dhiman R, Anand S, Reza-Garduno E, Cohen RE, McKinley GH, et al. Soft Matter 2013;9:1772–80.
[198] Schellenberger F, Xie J, Encinas N, Hardy A, Klapper M, Papadopoulos P, et al. Soft Matter 2015;11:7617–26.
[199] Wong T-S, Kang SH, Tang SKY, Smythe EJ, Hatton BD, Grinthal A, et al. Nature 2011;477:443–7.
[200] Epstein AK, Wong TS, Belisle RA, Boggs EM, Aizenberg J. Proc Natl Acad Sci U S A 2012;109:13182–7.
[201] Kim P, Kreder MJ, Alvarenga J, Aizenberg J. Nano Lett 2013;13:1793–9.
[202] Zhou XY, Zhang ZZ, Xu XH, Guo F, Zhu XT, Men XH, et al. ACS Appl Mater Interfaces 2013;5:7208–14.
[203] Wang N, Xiong DS, Deng YL, Shi Y, Wang K. ACS Appl Mater Interfaces 2015;7:6260–72.
[204] She ZX, Li Q, Wang ZW, Li LQ, Chen FA, Zhou JC. Chem Eng J 2013;228:415–24.
[205] Lu Y, Sathasivam S, Song JL, Crick CR, Carmalt CJ, Parkin IP. Science 2015;347:1132–5.
[206] Wang C-F, Wang T-F, Liao C-S, Kuo S-W, Lin H-C. J Phys Chem C 2011;115:16495–500.
[207] Zhang Y-L, Wang J-N, He Y, He Y, Xu B-B, Wei S, et al. Langmuir 2011;27:12585–90.
[208] Choi BG, Park HS. J Phys Chem C 2012;116:3207–11.
[209] Han D, Steckl AJ. Langmuir 2009;25:9454–62.
[210] Huang WH, Lin CS. Appl Surf Sci 2014;305:702–9.
[211] Kim TH, Ha SH, Jang NS, Kim J, Kim JH, Park JK, et al. ACS Appl Mater Interfaces 2015;7:5289–95.
[212] Seyfi J, Jafari SH, Khonakdar HA, Sadeghi GMM, Zohuri G, Hejazi I, et al. Appl Surf Sci 2015;347:224–30.
[213] Kumar KR, Ghosh SK, Khanna AS, Waghoo G, Ansari F, Yadav K. Dyes Pigments 2012;95:706–12.
[214] Hoshian S, Jokinen V, Somerkivi V, Lokanathan AR, Franssila S. ACS Appl Mater Interfaces 2015;7:941–9.
[215] Latthe SS, Sudhagar P, Devadoss A, Kumar AM, Liu SH, Terashima C, et al. J Mater Chem A 2015;3:14263–71.
[216] Wang HY, Liu ZJ, Wang EQ, Yuan RX, Gao D, Zhang XG, et al. Appl Surf Sci 2015;332:518–24.
[217] Mittal N, Deva D, Kumar R, Sharma A. Carbon 2015;93:492–501.
[218] Zhang HF, Yin L, Shi SY, Liu XW, Wang Y, Wang F. Microelectron Eng 2015;141:238–42.
[219] Huang JY, Li SH, Ge MZ, Wang LN, Xing TL, Chen GQ, et al. J Mater Chem A 2015;3:2825–32.
[220] Xue CH, Guo XJ, Ma JZ, Jia ST. ACS Appl Mater Interfaces 2015;7:8251–9.
[221] Xiang HF, Zhang L, Wang Z, Yu XL, Long YH, Zhang XL, et al. J Colloid Interface Sci 2011;359:296–303.
[222] Bayer IS, Fragouli D, Martorana PJ, Martiradonna L, Cingolani R, Athanassiou A. Soft Matter 2011;7:7939–43.
[223] Stamboulides C, Englezos P, Hatzikiriakos SG. Tribol Int 2012;55:59–67.
[224] Wan Y, Wang Z, Xu Z, Liu C, Zhang J. Appl Surf Sci 2011;257:7486–9.
[225] Brown PS, Bhushan B. J Colloid Interface Sci 2015;456:210–8.
[226] Wang L, Yang JY, Zhu Y, Li ZH, Sheng T, Hu YM, et al. Colloids Surf A Physicochem Eng Asp 2016;497:16–27.
[227] Bayer IS, Davis AJ, Loth E, Steele A. Mater Today Commun 2015;3:57–68.
[228] Davis A, Yeong YH, Steele A, Loth E, Bayer IS. AIChE J 2014;60:3025–32.
[229] Beckford S, Zou M. Appl Surf Sci 2013;292:350–6.
[230] Belova V, Gorin DA, Shchukin DG, Mohwald H. ACS Appl Mater Interfaces 2011;3:417–25.
[231] Wang RG, Kaneko J. Surf Eng 2013;29:255–63.
[232] Zhang XW, Hu LJ, Sun DZ. Acta Mater 2006;54:5469–75.
[233] Charitidis C, Gioti M, Logothetidis S, Kassavetis S, Laskarakis A, Varsano I. Surf Coat Technol 2004;180:357–61.
[234] Fang TH, Chang WJ, Lin CM. Microelectron Eng 2005;77:389–98.
[235] Beake BD, Leggett GJ. Polymer 2002;43:319–27.
[236] Miller M, Bobko C, Vandamme M, Ulm FJ. Cem Concr Res 2008;38:467–76.
[237] Saha R, Nix WD. Acta Mater 2002;50:23–38.
[238] Li XD, Bhushan B. Mater Charact 2002;48:11–36.
[239] Li X, Ding B, Lin J, Yu J, Sun G. J Phys Chem C 2009;113:20452–7.
[240] Jeong HE, Kwak MK, Park CI, Suh KY. J Colloid Interface Sci 2009;339:202–7.
[241] Lei W, Jia ZH, He JC, Cai TM. Appl Therm Eng 2014;62:507–12.
[242] Moulinet S, Bartolo D. Eur Phys J E 2007;24:251–60.
[243] McHale G, Shirtcliffe NJ, Newton MI. Langmuir 2004;20:10146–9.
[244] Murakami D, Jinnai H, Takahara A. Langmuir 2014;30:2061–7.
[245] Papadopoulos P, Mammen L, Deng X, Vollmer D, Butt H. Proc Natl Acad Sci U S A 2013;110:3254–8.
[246] Dorrer C, Ruhe J, Beilstein J. Nanotechnology 2011;2:327–32.
[247] Choi W, Tuteja A, Mabry JM, Cohen RE, GH McKinley. J Colloid Interface Sci 2009;339:208–16.
[248] Yan YY, Gao N, Barthlott W. Adv Colloid Interf Sci 2011;169:80–105.
[249] He Y, Jiang C, Yin H, Yuan W. Appl Surf Sci 2011;257:7689–92.
[250] Xiu Y, Zhu L, Hess DW, Wong CP. Nano Lett 2007;7:3388–93.